Generic modelling of non-perturbative quantities and a description of hard exclusive π^+ electroproduction

C. Bechler and D. Müller

Institut für Theoretische Physik II, Ruhr-Universität Bochum
D-44780 Bochum, Germany

Abstract

Based on Regge-inspired arguments and counting rules, we formulate empirical models for zero-skewness generalized parton distributions (GPDs) $\widetilde{H}^{(3)}$ and $\widetilde{E}^{(3)}$ in the iso-vector sector. If a hypothetical a_1/ρ_2 master trajectory is taken into account, we find that the polarized deep inelastic structure function $g_1^{(3)}$, axial-vector form factor, pseudoscalar form factor, and lattice data are well described. Thereby, we use a symmetric valence scenario in which the 'spin puzzle' in the iso-vector sector is trivially resolved. Utilizing a minimalist 'holographic' GPD principle, tying the t-channel angular momentum and collinear conformal spin together, we build skewness dependent GPD models. Confronting these models with HERMES and JLAB measurements of hard exclusive π^+ electroproduction within the collinear factorization approach, we might conclude that minimalist GPD models are disfavored at leading order. We provide then a set of GPDs on the cross-over line that fairly describes both HERMES and JLAB measurements.

Keywords: hard exclusive pion production, generalized parton distribution, generic modelling

PACS numbers: 12.38.Bx, 13.60.Le, 14.40.Cs

Contents

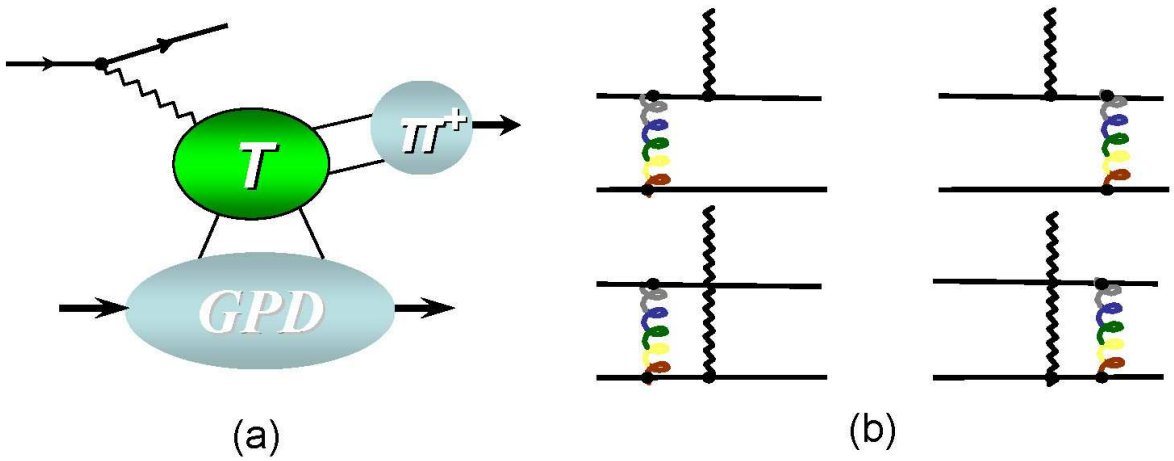

Figure 1: (a) Factorization of hard exclusive π^+ electroproduction at large photon virtuality $\mathcal{Q}^2$ into a hard-scattering amplitude T, the flavor changing generalized parton distribution, and pion distribution amplitude ϕ_π. (b) Hard scattering amplitude at leading order.

1 Introduction

The hard exclusive meson electroproduction off proton, e.g., for π^+

$$e^-(k)\, p(P_1) \to e^-(k')\, n(P_2)\, \pi^+(q_2)\,, \tag{1}$$

is considered as a promising channel to study the partonic content of the nucleon. If the proton is probed with a *longitudinal* polarized photon with sufficiently large virtuality $\mathcal{Q}^2 = -(k-k')^2$, the amplitude factorizes in a hard part, calculable in perturbation theory, and non-perturbative quantities that are universal, i.e., process independent, however, conventionally defined [1]. As illustrated in Fig. 1 (a), the virtual photon knocks out a quark-antiquark pair from the nucleon. In the collinear factorization framework the probability *amplitude* for this partonic process are the generalized parton distributions (GPDs), which depend on the longitudinal momentum fraction and a non-zero momentum flow in the t-channel [2, 3, 4]. The formation of the meson is described within a distribution amplitude (DA) [5, 6], i.e., the minimal Fock state component of the meson wave function, where the transverse distance of the quark-antiquark pair is squeezed.

The GPD framework is viewed as a powerful tool that provides insight in the partonic content of the nucleon and it ties perturbative and non-perturbative methods, for comprehensive reviews see Refs. [7, 8]. The hard exclusive processes, described to leading order (LO) accuracy, allow to access the GPDs on the cross-over line [9]. In particular, the hard exclusive photon electroproduction is widely considered as a theoretical clean process, see, e.g., Ref. [10] and references therein. The hard exclusive meson electroproduction, which might be utilized as a flavor filter, was elaborated at LO

accuracy for numerous channels [11, 12, 13, 14] and based on GPD models, estimates have been given, see, e.g., Refs. [15, 16, 17]. Perturbative next-to-leading order corrections were evaluated in Refs. [18, 19, 20], and power suppressed contributions were studied in Refs. [21, 22, 23, 24]. Model studies show that perturbative corrections are rather large, see also the comprehensive studies in Ref. [25]. Moreover, the factorization breaks down for power suppressed contributions and so a systematic expansion does not exist [1] and various helicity amplitudes with leading twist-three suffer from so-called end-point singularities [21].

The primary goal of revealing GPDs from the hard exclusive meson electroproducion is rather challenging for both experiment and theory. First, the cross section parts, which arise from longitudinal and transverse polarized photon exchange, must be separated. To apply the collinear factorization framework, the photon virtuality must be sufficiently large. Unfortunately, the onset of the perturbative framework is controversially discussed, where some considerations suggest that the perturbative description becomes reliable at a scale of $\mathcal{Q}^2 \gtrsim 10\,\mathrm{GeV}^2$. Such a scale is larger than the virtuality that is accessible in present fixed target experiments. We like to emphasize that the emission and absorbtion of a quark from the target resembles the Feynman mechanism and intuitively this might be considered as well describable. On the other hand the formation of the meson can be affected to a larger extent by power suppressed contributions, related to its transverse size. Relying on this picture, improvements have been suggested that provide models rather than a systematic framework.

For the hard exclusive electroproduction of a longitudinal polarized ρ^0_L meson it has been demonstrated that in a GPD framework, which contains also transverse degrees of freedom, experimental measurements can be described [15, 26, 27, 28]. In particular, at small x_B the model [27, 28], in which the GPD part is treated in the collinear approximation, successfully predicts the spin density matrix. However, from the success of such models one cannot draw conclusions about the collinear GPD approach, since model uncertainties are large and more importantly the interplay between perturbative and non-perturbative corrections in the collinear factorization approach and the transverse degrees of freedom is essentially not understood. To judge on the collinear factorization approach, one might confront theoretical "predictions" with experimental measurements. The problem of this approach is obvious, namely, one relies rather on a GPD model to reveal the GPD from experimental measurements. Thereby, the non-perturbative GPD models, not calculable from first principles, suffer from ad hoc assumptions, see, e.g., discussion in Ref. [29].

In this article we have a closer look to the phenomenological application of the GPD formalism to the hard exclusive π^+ electroproduction [14, 16, 18]. More specifically, we consider the

longitudinal photoproduction

$$\gamma_L^*(q_1)p(P_1) \to n(P_2)\pi^+(q_2) \tag{2}$$

within the collinear factorization approach at leading order of perturbation theory. We like to confront this approach with cross section measurements from the HERMES collaboration [30] and in HALL C at JLAB [31, 32]. In the later experiment the longitudinal cross section could be separated, however, both the energy and the photon virtuality are rather low. At the HERMES experiment a Rosenbluth separation cannot be performed. Fortunately, according to Regge-inspired model calculations [33, 34, 35], the pion pole enhances the longitudinal cross section at smaller values of $-t$ and it becomes the dominate part. We also include in our studies preliminary HERMES results for the single transverse proton spin asymmetry [36].

Our goal is to confront GPD models with measurements and to illuminate the interplay of model dependence and theoretical uncertainties. To set up our zero-skewness GPD models, we follow the idea, applied to polarized parton distribution functions (PDFs) [37], to constrain or reveal non-perturbative quantities from generic arguments. Our framework is set up in Mellin space and it allows us to skew the resulting models in a convenient way, where we utilize the t-channel SO(3) partial wave (PW) expansion [38, 39, 7].

The outline of the paper is as follows. In Sect. 2 we recall the perturbative framework for hard exclusive π^+ electroproduction at LO accuracy in the momentum fraction representation and then we present it in terms of conformal Mellin moments. In Sect. 3 we explore generic GPD modelling with Mellin moments, where we are guided by Regge-inspired arguments and counting rules. Thereby, we have to face the old problem that unnatural parity exchanges challenge Regge phenomenology. We will inspect the meson spectrum and we will argue that a odd J^{++} leading Regge trajectory might exist. As a side remark we shortly discuss the so-called 'spin puzzle' and we employ a symmetric valence matching scheme of collective and partonic degrees of freedom. Our zero-skewness GPD models are then introduced and we compare them with experimental measurements and lattice data. Relying on an ad hoc assumption, we set up a minimalist GPD model and inspect its properties. In Sect. 4 we shortly recall the illness of the perturbative framework and we utilize a scale setting prescription that might cure it. We provide then model predictions for the longitudinal cross section and single transverse proton spin asymmetry and confront them with HERMES and JLAB measurements. We will then take the point of view that an improved LO formalism is reliable and we present GPDs on the cross-over line that describe experimental data. Finally, we summarize and give our conclusions.

2 Collinear factorization approach at LO

We consider the hard exclusive π^+ electroproduction off a transverse polarized proton in the target rest-frame. More specifically, the z-axis is directed along the momentum of the virtual photon and both the azimuthal angles ϕ of the pion momentum and ϕ_S of the proton polarization vector are specified by the so-called Trento convention [40]. The cross section is straightforwardly evaluated in the collinear factorization approach to LO accuracy [1]. Thereby, the part of the cross section that arises from the exchange of a longitudinal polarized virtual photon is counted as the leading twist-two contribution. The exchange of a transverse polarized photon is on amplitude level formally suppressed by $1/\mathcal{Q}$ and will not be considered.

In the following we can safely neglect the pion mass and mass difference of proton and neutron, i.e., we set $M \equiv M_p = M_n$. In the twist expansion of the cross section we will adopt here the same conventions as used for the hard exclusive photon electroproduction in Ref. [41]. Namely, we decompose first the amplitude by inserting photon helicity states into a leptonic and hadronic part. We exactly calculate the leptonic part and drop any power suppressed contribution in the hadronic part. Thereby, we choose $1/\mathcal{Q}$ as expansion parameter and the Bjorken variable $x_{\rm B} = \mathcal{Q}^2/(2q_1 \cdot P_1)$ as scaling variable. Finally, we can write the differential cross section for hard exclusive π^+ electroproduction, induced by longitudinal polarized photon exchange, at twist-two level as

$$\frac{d\sigma^{\pi^+}}{d\mathcal{Q}^2 dx_{\rm B} dt d\varphi} \overset{\rm Tw-2}{=} \frac{\alpha_{\rm em}^2}{\mathcal{Q}^8} \frac{\varepsilon\, y^2}{1-\varepsilon} \frac{x_{\rm B}}{\sqrt{1+\epsilon^2}} \Bigg\{ (1-\xi^2)|\widetilde{\rm H}_{\pi^+}|^2 - \frac{t}{4M^2}|\xi\widetilde{\rm E}_{\pi^+}|^2 - 2\xi^2 \Re{\rm e}\left(\widetilde{\rm H}_{\pi^+}\widetilde{\rm E}^*_{\pi^+}\right) \\ -2\sin(\phi-\phi_S)\sqrt{\frac{t-t_{\rm min}}{t_{\rm min}}}\,\xi^2\,\Im{\rm m}\left(\widetilde{\rm H}_{\pi^+}\widetilde{\rm E}^*_{\pi^+}\right) \Bigg\}\Bigg|_{\xi\to\frac{x_{\rm B}}{2-x_{\rm B}}} . \tag{3}$$

Here $y = q_1 \cdot P_1/k \cdot P_1$ is the photon energy momentum fraction, $t = (P_2 - P_1)^2$ is the squared momentum transfer, the symmetric scaling variable ξ is consequently replaced by $x_{\rm B}/(2-x_{\rm B})$, and $\epsilon = x_{\rm B}M/\mathcal{Q}$ is a shorthand. The polarization parameter

$$\varepsilon = \frac{1 - y - \frac{1}{4}y^2\epsilon^2}{1 - y + \frac{1}{2}y^2 + \frac{1}{4}y^2\epsilon^2} \tag{4}$$

is the ratio of longitudinal and transverse photon flux. The minimal value of $-t$ is

$$-t_{\rm min} = \mathcal{Q}^2 \frac{2(1-x_{\rm B})(1-\sqrt{1+\epsilon^2})+\epsilon^2}{4x_{\rm B}(1-x_{\rm B})+\epsilon^2} \approx \frac{M^2 x_{\rm B}^2}{1-x_{\rm B}} , \tag{5}$$

where the indicated approximation is valid for $x_{\rm B}M^2/\mathcal{Q}^2 \ll 1-x_{\rm B}$. The hadronic part is contained in the *transition form factors* (TFFs) $\widetilde{\rm H}_{\pi^+}$ and $\widetilde{\rm E}_{\pi^+}$. They might be viewed as physical quantities that depend on the symmetric scaling variable ξ, t, and $\mathcal{Q}^2$.

As depicted in Fig. 1a, the TFF $\widetilde{\mathrm{H}}_{\pi^+}$ ($\widetilde{\mathrm{E}}_{\pi^+}$) factorizes into a convolution of a hard amplitude T_{ud} with the GPD $\widetilde{H}^{ud}$ ($\widetilde{E}^{ud}$) and the pion DA ϕ_π[1]:

$$\left\{\begin{matrix}\widetilde{\mathrm{H}}_{\pi^+}\\ \widetilde{\mathrm{E}}_{\pi^+}\end{matrix}\right\} = \int_0^1 du \int_{-1}^1 dx\ \phi_\pi(u,\mu^2) T_{ud}\left(u,x,\xi|\alpha_s(\mu_r^2),\mathcal{Q}^2/\mu^2,\mathcal{Q}^2/\mu_r^2\right) \left\{\begin{matrix}\widetilde{H}^{ud}\\ \widetilde{E}^{ud}\end{matrix}\right\}\left(x,\xi,t|\mu^2\right) + \dots\,, \quad (6)$$

where the ellipsis stands for power suppressed contributions. Here, we distinguish between the renormalization scale μ_r and the factorization scale μ. Note that the truncation of the perturbation series induces residual scale dependence. The $\widetilde{H}^{ud}$ and $\widetilde{E}^{ud}$ GPDs, depending on the quark momentum fraction x, ξ, t, and μ, are flavor non-diagonal and parity-odd. They are defined by a form factor decomposition of light-ray operator matrix elements in the standard notation, see, e.g., Ref. [18]. The leading twist-two pion DA ϕ_π, depending on the quark momentum fraction u and factorization scale μ, is conventionally normalized to the pion decay constant:

$$\int_0^1 du\, \phi_\pi(u,\mu^2) = f_\pi\,, \quad f_\pi \simeq 133\,\mathrm{MeV}\,. \quad (7)$$

The short-distance dynamics, i.e., the hard amplitude T_{ud}, can be perturbatively calculated as a series in the strong coupling $\alpha_s(\mu_r)$, known to NLO accuracy [18]. From the tree diagrams, presented in Fig. 1b, we recover the well known result [14, 16, 15]:

$$T_{ud}(u,x,\xi|\alpha_s(\mu_r^2),\mathcal{Q}^2/\mu^2,\mathcal{Q}^2/\mu_r^2) = \frac{C_F}{N_c}\alpha_s(\mu_r^2)\left\{\frac{Q_u}{(1-u)\,(\xi-x-i0)} - \frac{Q_d}{u\,(\xi+x-i0)}\right\} + \mathcal{O}(\alpha_s^2)\,, \quad (8)$$

where $C_F = 4/3$, $N_c = 3$, and the fractional quark charges are $Q_u = 2/3$ and $Q_d = -1/3$. The hard amplitude (8) is proportional to the running coupling

$$\alpha_s(\mu_R^2) = \frac{4\pi}{\beta_0 \ln\frac{\mu_R^2}{\Lambda^2_{\mathrm{QCD}}}} \quad \text{with} \quad \beta_0 \equiv 11 - 2n_f/3 = 9\,, \quad (9)$$

where we set n_f, the number of active quarks, to three and in the following we will take the QCD scaling parameter $\Lambda_{\mathrm{QCD}} = 200$ MeV. We emphasize that in principle the renormalization scale μ_R can be ambiguously chosen because this ambiguity is annulled in the full perturbative series.

In the following we will stay at LO accuracy and equate the factorization scale with the photon virtuality, i.e., we set $\mu^2 = \mathcal{Q}^2$. In the LO approximation the hard amplitude (8) possesses a factorized u and $\xi \mp x$ momentum fraction dependence[1]. Since the pion DA has definite charge parity-even, possessing the symmetry $\phi_\pi(u) = \phi_\pi(1-u)$, the convolution integral

$$\mathcal{I}_\pi(\mathcal{Q}^2) = \frac{1}{3f_\pi}\int_0^1 du\,\frac{\phi_\pi(u,\mathcal{Q}^2)}{u}, \quad (10)$$

[1]Note that although NLO corrections might be rather large, it is expected that this factorization is only slightly spoiled by radiative NLO corrections, see, e.g., Ref. [42].

enters as overall factor in the normalization of the TFFs (6). The value of the inverse moment (10) is directly 'measurable' at LO accuracy in the fusion process $\gamma^*\gamma \to \pi^0$ [5]. The factorized GPD part of the $\widetilde{\mathrm{H}}^{ud}$ and $\widetilde{\mathrm{E}}^{ud}$ TFFs (6) might be decomposed in terms with definite charge parity,

$$\widetilde{H}^{ud\pm}(x,\cdots) = \widetilde{H}^{ud}(x,\cdots) \pm \widetilde{H}^{ud}(-x,\cdots)\,, \quad \widetilde{E}^{ud\pm}(x,\cdots) = \widetilde{E}^{ud}(x,\cdots) \pm \widetilde{E}^{ud}(-x,\cdots)\,. \quad (11)$$

Here the $\pm$ superscript refers in the first place to the symmetry behavior under $x \to -x$ and it coincides for both of our parity-odd GPDs with the t-channel charge parity $C = \pm 1$. Employing isospin symmetry, one can express the flavor off-diagonal GPDs to the common flavor diagonal ones in the iso-vector sector [13]:

$$\widetilde{H}^{ud} = \widetilde{H}^{(3)} \equiv \widetilde{H}^{u} - \widetilde{H}^{d}\,, \quad \widetilde{E}^{ud} = \widetilde{E}^{(3)} \equiv \widetilde{E}^{u} - \widetilde{E}^{d}\,. \quad (12)$$

The convolution of these GPDs with the LO hard scattering kernel

$$\mathcal{F}(\xi,t,\mathcal{Q}^2) \stackrel{\mathrm{LO}}{=} \int_{-1}^{1} dx\, \frac{F(x,\xi,t,\mathcal{Q}^2)}{\xi - x - i0}\,, \quad \mathcal{F}(F) = \left\{\widetilde{\mathcal{H}}^{ud\pm}(\widetilde{H}^{ud\pm}), \widetilde{\mathcal{E}}^{ud\pm}(\widetilde{E}^{ud\pm})\right\} \quad (13)$$

might be denoted as 'Compton form factors' ('CFFs'). Note, however, that only the charge even part (plus superscript) enters in the LO approximation of the deeply virtual Compton scattering (DVCS) amplitude. In the case of hard exclusive π^+ production we have the combination

$$\begin{Bmatrix} \widetilde{\mathcal{H}}^{ud} \\ \widetilde{\mathcal{E}}^{ud} \end{Bmatrix} = \begin{Bmatrix} \widetilde{\mathcal{H}}^{(3)+} + \frac{1}{6}\widetilde{\mathcal{H}}^{(3)-} \\ \widetilde{\mathcal{E}}^{(3)+} + \frac{1}{6}\widetilde{\mathcal{E}}^{(3)-} \end{Bmatrix} \quad (14)$$

in which also the charge even part dominates. Putting all definitions together, we finally have a very compact LO expression for the TFFs

$$\begin{Bmatrix} \widetilde{\mathrm{H}}_{\pi^+} \\ \widetilde{\mathrm{E}}_{\pi^+} \end{Bmatrix} (\xi,t,\mathcal{Q}^2) \stackrel{\mathrm{LO}}{=} \alpha_s(\mu_r^2)\frac{2f_\pi}{3}\mathcal{I}_\pi(\mathcal{Q}^2) \begin{Bmatrix} \widetilde{\mathcal{H}}^{(3)+} + \frac{1}{6}\widetilde{\mathcal{H}}^{(3)-} \\ \widetilde{\mathcal{E}}^{(3)+} + \frac{1}{6}\widetilde{\mathcal{E}}^{(3)-} \end{Bmatrix} (\xi,t,\mathcal{Q}^2) + \cdots\,. \quad (15)$$

Here the renormalization scale is ambiguous and so $\alpha_s(\mu_r^2)$ might be loosely viewed as an "effective charge". As we will argue below in Sect. 4, its value might be extracted from the measurement of the pion form factor. Let us emphasize that in principle Eq. (15) can serve as a *qualitative* test of the collinear factorization approach, where the TFFs of hard exclusive π^+ electroproduction are expressed in terms of quantities that can be addressed in the LO approximation of the pion-to-photon transition form factor, pion form factor, and to a certain extent in DVCS.

Let us also introduce the conformal PW expansion of the TFFs. The underlying symmetry is the collinear conformal group SL(2,$\mathbb{R}$) and in pQCD it can be used to diagonalize the evolution equation, see, e.g., Ref. [43]. The conformal PW expansion for the pion DA is well known at LO [5, 6],

$$\phi_\pi(v,\mathcal{Q}^2) = f_\pi \sum_{\substack{n=0 \\ \text{even}}}^{\infty} 6(1-v)vC_n^{3/2}(2v-1)\,\mathbb{E}_n(\mathcal{Q},\mathcal{Q}_0)a_n(\mathcal{Q}_0^2)\,, \quad (16)$$

where the conformal PWs are given in terms of orthogonal Gegenbauer polynomials C_n^ν of order n and index $\nu = 3/2$. The partonic "quantum number", conjugated to the momentum fraction u is the (integral) conformal spin $n+2$. The first coefficient $a_0 = 1$ is fixed by the normalization (7) and does not evolve, i.e., $\mathbb{E}_0(\mathcal{Q}, \mathcal{Q}_0) = 1$. If the scale $\mathcal{Q} > \mathcal{Q}_0$ increases, the evolution operator

$$\mathbb{E}_n(\mathcal{Q}, \mathcal{Q}_0) = \left(\frac{\ln(\mathcal{Q}^2/\Lambda^2_{\rm QCD})}{\ln(\mathcal{Q}_0^2/\Lambda^2_{\rm QCD})}\right)^{-\gamma_n^{(0)}/\beta_0}, \quad \gamma_n^{(0)} = \frac{4}{3}\left(4S_{n+1} - \frac{2}{(n+1)(n+2)} - 3\right), \tag{17}$$

reduces the magnitude of conformal moments a_n with $n > 0$. Here the harmonic sum is defined as $S_m = \sum_{k=1}^m \frac{1}{k}$. The inverse moment, given in Eq. (10) as convolution integral, might be now expressed as a series of conformal moments

$$\mathcal{I}_\pi(\mathcal{Q}^2) = \sum_{\substack{n=0\\ \text{even}}}^{\infty} \mathbb{E}_n(\mathcal{Q}, \mathcal{Q}_0) a_n(\mathcal{Q}_0^2)\,. \tag{18}$$

For the t-channel crossed GPDs, i.e., the so-called generalized DAs, one might write down an analogous conformal PW expansion as in Eq. (16). The conformal moments of a quark GPD are group theoretically defined in terms of Gegenbauer polynomials $C_j^{3/2}$ of order j and with index $\nu = 3/2$:

$$\left\{\begin{array}{c}\widetilde{H}_j\\ \widetilde{E}_j\end{array}\right\}(\eta, t, \mathcal{Q}^2) = \frac{\Gamma(3/2)\Gamma(1+j)}{2^{j+1}\Gamma(3/2+j)} \int_{-1}^1 dx\, \eta^j C_j^{3/2}(x/\eta) \left\{\begin{array}{c}\widetilde{H}\\ \widetilde{E}\end{array}\right\}(x, \eta, t, \mathcal{Q}^2)\,. \tag{19}$$

Note that our definition ensures that [anti]symmetric functions possesses only even [odd] integral moments, which are even polynomials in η of order j [or $j-1$]. In the limit $\eta \to 0$ the conformal moments of $\widetilde{H}$ GPD coincide with the Mellin moments of a polarized PDF:

$$\widetilde{H}_j^\pm(\eta = 0, t, \mathcal{Q}^2) = \frac{1 \pm (-1)^j}{2} \int_0^1 dx\, x^j \widetilde{H}_j^\pm(x, \eta = 0, t, \mathcal{Q}^2)\,. \tag{20}$$

As in the case of a SO(3) PW expansion, labelled by the t-channel angular momentum, such a series does not converge for the s-channel analog. We can borrow us the known recipes and employ a Sommerfeld-Watson transform [44], which reads for the 'CFFs' as follows

$$\left\{\begin{array}{c}\widetilde{\mathcal{H}}\\ \widetilde{\mathcal{E}}\end{array}\right\}^\pm \overset{\rm LO}{=} \frac{1}{2i}\int_{c-i\infty}^{c+i\infty} dj\, \frac{\Gamma(5/2+j)}{\Gamma(3/2)\Gamma(3+j)} (\xi/2)^{-j-1} \mathbb{E}_j(\mathcal{Q}, \mathcal{Q}_0) \frac{\mp 1 - e^{-i\pi j}}{\sin \pi j} \left\{\begin{array}{c}\widetilde{H}_j\\ \widetilde{E}_j\end{array}\right\}^\pm (\xi, t, \mathcal{Q}_0^2)\,. \tag{21}$$

The analytic continuation of the evolution operator is straightforward by replacing $n \to j$ and representing the harmonic sum $S_{j+1} = \psi(j+2) - \psi(1)$ in terms of Euler's ψ functions. The analytic continuation of integral conformal GPD Mellin moments (19), is dictated by the requirement that after crossing $\xi \to 1/\xi$, the Mellin-Barnes integral yields a series, rather similar to the convolution integral (18). In general this requires a separate continuation of even and odd conformal moments.

3 Generic modelling in Mellin space

A GPD $F(x,\eta,t)$ at a given input scale μ^2 is an intricate function of three variables, the s-channel momentum fraction x, its t-channel counterpart $\eta \sim (P_1 - P_2)_+$, and t. With the growing amount of experimental data for the hard exclusive photon electroproduction it became obvious that popular ad hoc GPD models do not posses predictive power on quantitative level; a more detailed discussion can be found in Ref. [29]. For our purpose, namely, a qualitative confrontation of the collinear factorization approach with hard exclusive π^+ electroproduction measurements, it is sufficient to deal with zero-skewness GPD models and an ad hoc prescription to skew them. In the following we work with conformal GPD Mellin moments (19), which in principle allows us to set up flexible GPD models.

To parameterize the η-dependence of GPDs, we follow Ref. [38] and expand the conformal moments (19) in terms of t-channel SO(3) PWs. These PWs are given in terms of the Wigner rotation matrices $d^J_{0,0}(\cos\theta)$ and $d^J_{0,1}(\cos\theta)$, i.e., by Legendre or Gegenbauer polynomials, respectively [7, 45]. Here the second subscript refers to the helicity difference of the final state $N^{\uparrow(\downarrow)}\bar{N}^{\uparrow}$ in the t-channel center-of-mass frame, i.e., for (anti-)aligned nucleon helicities it is zero (one). The center-of-mass scattering angle θ is approximatively related to the skewness parameter $\eta \approx -1/\cos\theta$. Note that the exact relation would yield more cumbersome formulae that provide no advantages or improvements for our GPD modelling. The crossed version of the Wigner rotation matrices are noted for shortness as $\hat{d}^J_{0,0}(\eta)$ and $\hat{d}^J_{0,1}(\eta)$ and they are normalized in the limit $\eta \to 0$ to one [45]. Their analytic continuation with respect to the t-channel angular momentum J is defined in the traditional way and we express them by hypergeometric functions:

$$\hat{d}^J_{0,1}(\eta) = \frac{\Gamma(3/2)\Gamma(2+J)}{2^J\Gamma(1/2+J)}\,\eta^{J-1}\,{}_2F_1\left(\begin{matrix}-J+1, J+2\\ 2\end{matrix}\Big|\frac{\eta-1}{2\eta}\right), \tag{22}$$

$$\hat{d}^J_{0,0}(\eta) = \frac{\Gamma(1/2)\Gamma(1+J)}{2^J\Gamma(1/2+J)}\,\eta^{J}\,{}_2F_1\left(\begin{matrix}-J, J+1\\ 1\end{matrix}\Big|\frac{\eta-1}{2\eta}\right). \tag{23}$$

Now we can straightforwardly write down the SO(3)-PW expansion for integral conformal GPD moments (19). For the target helicity conserved GPD $\widetilde{H}$ the SO(3)-PW expansion reads

$$\widetilde{H}^{\pm}_j(\eta,t) = \sum_{J=1}^{j+1} \frac{1 \mp (-1)^J}{2} \widetilde{H}^{\pm}_{jJ-1}(t)\,\eta^{j+1-J}\,\hat{d}^J_{0,1}(\eta)\,. \tag{24}$$

Here even j moments (plus superscript) and odd j moments (minus superscript) are build up by odd J^{++} and even J^{--} exchanges, respectively [39, 7]:

$$J^{\rm PC} = 1^{++}, 3^{++}, \cdots, (j+1)^{++}, \quad J^{\rm PC} = 2^{--}, 4^{--}, \cdots, (j+1)^{--}\,. \tag{25}$$

Note that here the difference $j-J$ is always odd and so a confusion with the notion signature, which might be used in both the conformal and SO(3) PW expansion, could appear. We consequently

stick here and in the following to the Regge terminology and associate signature plus and minus with even and odd J, respectively.

The t-channel helicity conserved GPD moments are expressed by a combination of s-channel flip and non-flip contributions:

$$\left[\widetilde{H}_j^{\pm} + \frac{t}{4M^2}\widetilde{E}_j^{\pm}\right](\eta,t) = \sum_{J=0}^{j} \frac{1\pm(-1)^J}{2}\left[\widetilde{H}'^{\pm}_{jJ}(t) + \frac{t}{4M^2}\widetilde{E}^{\pm}_{jJ}(t)\right]\eta^{j-J}\,\hat{d}^J_{0,0}(\eta)\,. \tag{26}$$

Now the even j moments (plus superscript) and odd j moments (minus superscript) are associated with even J^{-+} and odd J^{+-} t-channel exchanges, respectively [39, 7]:

$$J^{\rm PC} = 0^{-+},\, 2^{-+},\, \cdots,\, j^{-+}\,, \quad J^{\rm PC} = 1^{+-},\, 3^{+-},\, \cdots,\, j^{+-}\,. \tag{27}$$

We might utilize the crossed version of Wigner's rotation matrices $\hat{d}^J_{0,0}(\eta)$ within the assignment (27) in the SO(3) PW expansion of $\widetilde{E}$ GPD conformal moments:

$$\widetilde{E}_j^{\pm}(\eta,t) = \sum_{J=0}^{j} \frac{1\pm(-1)^J}{2}\widetilde{E}^{\pm}_{jJ}(t)\,\eta^{j-J}\,\hat{d}^J_{0,0}(\eta)\,. \tag{28}$$

Then the $\widetilde{H}$ GPD conformal moments can be alternatively represented by the SO(3) PW expansion (24) and (26) in terms of the amplitudes $\widetilde{H}_{j,J-1}(t)$ and $\widetilde{H}'_{jJ}(t)$, respectively. Consequently, these both PW amplitudes can be mapped to each other. Below we will assume that the $\widetilde{H}_j$ conformal moments are only built by one leading SO(3) PW $J = j+1$ with odd J^{++} or even J^{--}. This implies that all PW amplitudes of $\widetilde{H}'_{jJ}(t)$, appearing in Eq. (26) and containing contributions from even J^{-+} or odd J^{+-} exchanges, are exited. Of course, they can be entirely expressed in terms of $\widetilde{H}_{j,j}(t)$ amplitudes:

$$\widetilde{H}'_{jJ}(t) = \frac{\Gamma(J+3/2)\Gamma(j+1)}{2^{J-j}\Gamma(j+3/2)\Gamma(J+1)}\widetilde{H}_{jj}(t)\,, \quad j \geq J \geq 0\,. \tag{29}$$

In the following sections we model the zero-skewness Mellin moments,

$$\widetilde{H}_j^{(3)}(\eta=0,t) = \widetilde{H}_{jj}^{(3)}(t) \quad \text{and} \quad \widetilde{E}_j^{(3)}(\eta=0,t) = \widetilde{E}_{jj}^{(3)}(t),$$

in the iso-vector sector. Although Regge theory is developed for on-shell scattering, it is obvious from the phenomenology that *effective* Regge behavior also appears in off-shell amplitudes. As a fact of matter, in the collinear factorization approach *effective* Regge behavior is encoded in PDFs, obtained from global fits, and so also in GPD models. Moreover, it is rather robust under evolution, except for the "pomeron"-like exchange [46]. Hence, Regge poles should be a building block for our partonic SO(3) PW amplitudes. The corresponding PW amplitudes will be interpreted according to Regge phenomenology and they are in the t-channel, i.e., $\gamma_L^*\pi^- \to n\bar{p}$, given by exchanges with

definite J. Analogous as in Regge theory, applied to high-energy on-shell scattering, this allows us to resum t-channel exchanges and, finally, they determine the small-x behavior of GPDs or PDFs. Moreover, a link between *effective* Regge behavior and t-dependence of nucleon form factors has been also employed or observed in zero-skewness GPD models [47, 48, 44]. We are going along the line of Ref. [44, 45, 49] and unpublished work, shortly mentioned in Ref. [50] (see corresponding talk at DIS2008). There the t-dependence of H and E GPD Mellin moments is modelled as a product of leading and daughter Regge poles. Since the empirical H and E GPD models describe within generic numbers, obtained from counting rules and Regge theory, form factors, unpolarized PDFs, and lattice data, we are encouraged to utilize generic modelling in the following sections.

However, first we have a look to the phenomenological status of Regge trajectories in the meson spectrum. We then build our zero-skewness GPD models and confront them with the polarized deep inelastic scattering (DIS) structure function g_1, form factor measurements, and lattice data. Finally, we skew our GPD models within a *minimalist* prescription as they arise from the dominance of the leading SO(3) PW in the expansion (24) and (28). We also discuss the model properties, relevant for the phenomenology of hard exclusive π^+ electroproduction.

3.1 Regge trajectories from meson spectroscopy

According to the quantum numbers (25) and (27), we are dealing with unnatural parity

$$P = -(-1)^J$$

t-channel exchanges such as π_0^{-+}/b_1^{+-} and a_1^{++}/ρ_2^{--} ones. Such exchanges challenge Regge phenomenology, applied to high energy on-shell scattering processes, see reviews [52, 53]. We are not aware that the problems there, e.g., an unexpected large a_1 pole contribution in $\pi^- p \to \rho^0 n$ [52], were finally solved, e.g., in terms of very large Regge cut contributions. Therefore, and because of the immense experimental progress in meson spectroscopy during the last decade, see the comprehensive reviews [54, 55], it is worth to have a fresh look to Regge trajectories in the meson spectrum. Thereby, we take experimental data from the Particle Data Group (PDG) [51], where we also include mesons listed under further states.

According to Eq. (25), the leading SO(3) PW amplitudes $\widetilde{H}_{jj}^{(3)+}$ and $\widetilde{H}_{jj}^{(3)-}$ with even and odd $j = J - 1$, respectively, carry odd J^{++} and even J^{--} t-channel quantum numbers. We associate them with meson exchanges that belong to a_1 and ρ_2 trajectories. In the Chew-Frautschi plot in Fig. 2 the iso-vector mesons

$$a_1, \;\; a_3, \;\; \rho_2 \;\; \text{and} \;\; \rho_4$$

might lie on trajectories, which we traditionally consider as linear equidistantly spaced, i.e.,

$$J(M^2) = \alpha^{(n)}(M^2)\,, \quad \alpha^{(n)}(M^2) \simeq \alpha_0 - n + \alpha' M^2\,, \quad n = 0, 1, 2, \cdots\,, \tag{30}$$

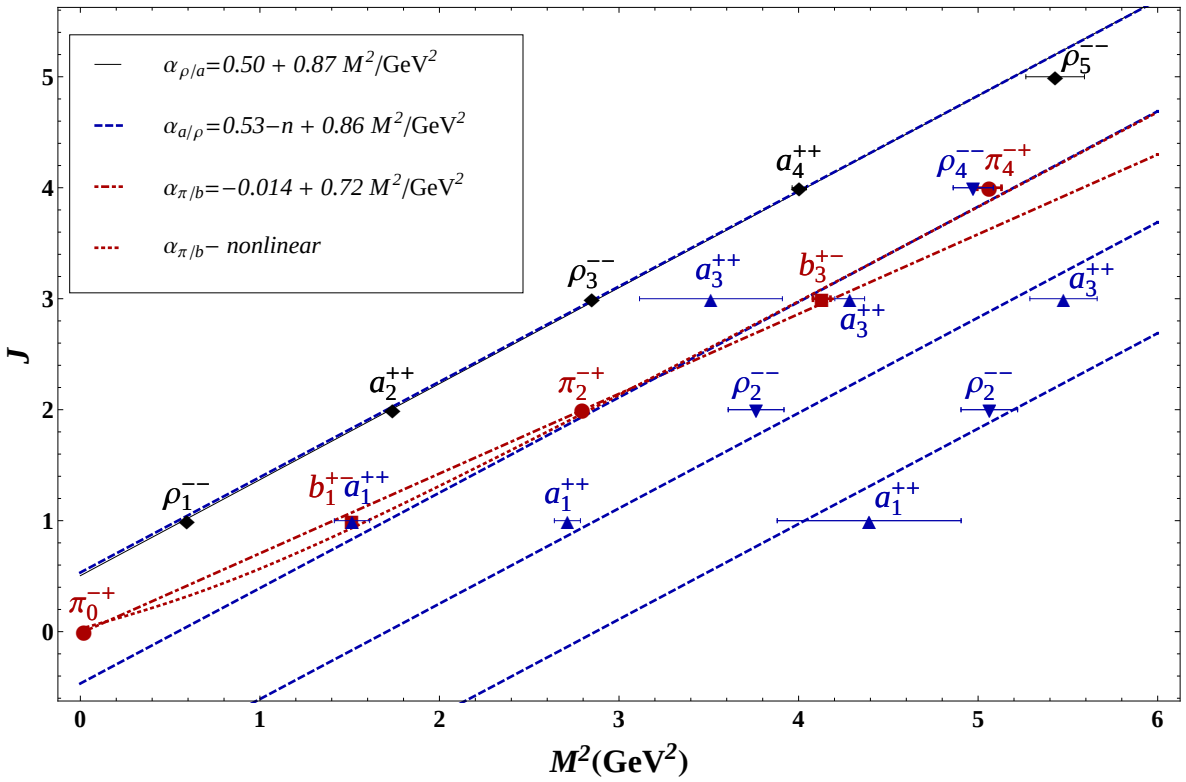

Figure 2: Spectrum of iso-vector mesons a_1, a_3, ρ_2 and ρ_4, the states of the leading π_0/b_1 and ρ_1/a_2 trajectories. Curves show linear Regge trajectory fits, a_1/ρ_2 (dashed), π_0/b_1 (dot-dashed) and $\rho_1/a2$ (solid), and an example of a non-linear π_0/b_1 trajectory (dotted). Spectroscopic data are from the Review of Particle Physics [51].

where $\alpha(M^2) \equiv \alpha^{(n=0)}(M^2)$ is called master trajectory. In particular, the states

$$a_1(1260)[1230 \pm 40], \quad a_3(2070)[2070 \pm 30], \quad \rho_4(2240)[2230 \pm 25]$$

[values in square brackets are the mass and its error in MeV, quoted by the PDG] might belong to the trajectory with the largest intercept, called a_1 trajectory. Note however, that ρ_2 is not established and

$$a_3(1875)[1874 \pm 43 \pm 96]$$

lies between the ρ_1/a_2 master and the a_1 trajectory within an equal distance of slightly more than 1-σ standard deviation (errors are added in quadrature). The states $a_1(1640)$, $\rho_2(1940)$, $a_3(2310)$ and $a_1(2095)$, $\rho_2(2240)$ might belong to two daughter trajectories.

Let us first suppose that both states $a_3(1875)$ and $a_3(2070)$ nearly belong to the a_1 trajectory. A least square fit within a linear a_1 trajectory and two daughters reveals that $\chi^2/\text{d.o.f.} \approx 4.1/(9-2)$ does not contradict our hypothesis and the result

$$\alpha^{\text{est}}_{a_1}(s) = -(0.32 \pm 0.30) + (0.83 \pm 0.07)\ s/\text{GeV}^2\,, \qquad \chi^2/\text{d.o.f.} \approx 0.59 \tag{31}$$

confirms the a_1 trajectory that is *"established"* in the literature. The trajectory (31) has a typical t-slope and its intercept $-0.6 \lesssim \alpha_{a_1}(0) \lesssim 0$ suffers from a large uncertainty. Such an uncertainty appears also in the analyzes of high-energy scattering processes, see, e.g., discussion in Ref. [56].

Certainly, other interpretations of the a_J meson spectrum are not excluded, e.g., one might consider the a_1 trajectory as degenerated with a non-linear π_0 trajectory [57], as illustrated by the dotted curve in Fig. 2. Also it has been argued that chiral symmetry might be partially restored at large J, and so *exotic* parity doubling[2] appears in the meson spectrum, see review [58]. According to that, at sufficiently large J a meson with natural parity, belonging to the master trajectory, should posses two partners with unnatural parity. The author of Ref. [59] argued that the $\rho_3^{--}(1690)$ meson has a $3^{++}(\sim 1700)$ partner. The large mass error allows us to speculate that $a_3^{++}(1875)$, reported in 2002 in Ref. [60], is a parity doubling candidate, which might indicate a partial chiral symmetry restoration.

We now count the $a_3^{++}(1875)$ state to a master trajectory and like to know whether it is degenerated with the ρ_1/a_2 trajectory. A fit to the a_1/ρ_2 meson spectrum yields the result

$$\alpha^{(n)}_{a_1/\rho_2}(s) = (0.53 \pm 0.34) - n + (0.86 \pm 0.08)\ s/\mathrm{GeV}^2\,, \qquad \chi^2/\mathrm{d.o.f.} \approx 0.67\,, \tag{32}$$

which is with $n = 1$ fully compatible with the previous one (31). Although the uncertainty is large, the means somehow suggest that this trajectory is degenerated with the ρ_1/a_2 one. In Fig. 2. our fit result (32), shown as dashed curve, is hardly to distinguish from the ρ_1/a_2 master trajectory (solid curve), which we obtained from a separate fit to its first five members.

Further support for the existence of a master a_1/ρ_2 trajectory arises from polarized DIS. Here, the rise of the iso-vector polarized nucleon structure function $g_1^{(3)}(x_\mathrm{B})$ at small-x_B might be viewed as a $x_\mathrm{B}^{-\lambda}$ power behavior with $\lambda \sim 1/2$ [61, 62], illustrated below in the left panel of Fig. 3. Such a power behavior, partly even a stronger one, is included in standard PDF parameterizations and it is predicted by a double log resummation [63]. On the other hand in the Regge framework, one equates $\lambda = \alpha_{a_1}(0)$ [64]. Hence, from the *"established"* a_1 trajectory (31) it is then expected that $g_1^{(3)}(x_\mathrm{B})$ in the small-x_B region vanishes or approaches a constant, which contradicts experimental measurements. As the authors of Refs. [61, 62], we are not aware that this Regge puzzle is solved.

Although it is not conclusive from the meson spectrum that a leading trajectory for unnatural parity states exists, we conjecture a master a_1/ρ_2-trajectory,

$$\alpha_{a_1/\rho_2}(s) \cong \alpha_{\rho_1/a_2}(s) = (0.5 \pm 0.05) + (0.87 \pm 0.05)\, s/\mathrm{GeV}^2\,, \qquad \chi^2/\mathrm{d.o.f.} = 0.24\,, \tag{33}$$

[2] Using $J = \alpha^{(n)}(M^2)$ and the assignment $P = (-1)^{L+1}$ and $C = (-1)^{L+S}$, where according to the quark model $S = \{0, 1\}$, it is easy to see that a parity doubling *pattern* appears in the meson spectrum, except for the master trajectory $\alpha_{\rho_1/a_2}(M^2)$ itself. Partial restoration of chiral symmetry predicts that parity $(-1)^J$ states on the ρ_1/a_2 master trajectory at sufficiently large J are degenerated with two further parity $(-1)^{J+1}$ states, carrying $C = +1$ and $C = -1$, respectively.

to explain the rise of the polarized DIS structure function $g_1^{(3)}$. We consider this hypothetic Regge trajectory as degenerated with the master ρ_1/a_2-trajectory and we view the *"established"* a_1-trajectory as its first daughter. We did not investigate whether our conjecture resolves problems or contradicts phenomena in on-shell processes at high energy [52, 53].

We inspect now the even J^{-+} and odd J^{+-} Regge trajectories that appear in the SO(3) PWs of $\widetilde{E}^+_{jj}$ and $\widetilde{E}^-_{jj}$, respectively, where $j = J$, see Eq. (27). Presumably, the leading trajectories are non-linear and their daughters are populated with natural parity vector states π_1^{-+}, having exotic quark model quantum numbers ($S = 0$ and even L). Since this is not compatible with our hypothesis (30), we do not utilize daughter trajectories. The leading signature even and odd trajectory are populated with

$$\pi_0^\pm\,[(139.57018 \pm 0.00035)\,\mathrm{MeV}]\,, \quad \pi_2(1670)\,[(1672.4 \pm 3.2)\,\mathrm{MeV}]\,, \quad \pi_4(2250)\,[(2250 \pm 15)\,\mathrm{MeV}]$$

and

$$b_1(1235)\,[(1229.5 \pm 3.2)\,\mathrm{MeV}]\,, \quad b_3(2025)\,[(2032 \pm 12)\,\mathrm{MeV}]$$

mesons, respectively.

If we ignore the $\pi_4(2250)$ state, reported in 2001 in Ref. [65], and we assume that the trajectories are linear and degenerated, we find from a fit the π_0/b_1-trajectory

$$\alpha_{\pi_0/b_1}(s) = (-0.014 \pm 0.002) + (0.72 \pm 0.01)\,s/\mathrm{GeV}^2\,, \qquad \chi^2/\mathrm{d.o.f.} \approx 1.1\,, \tag{34}$$

shown in Fig. 2 as dot-dashed line. Since this trajectory is often used, we denote it as *"established"*. Compared to a typical meson Regge trajectory, the *"established"* π_0/b_1-trajectory has a smaller slope parameter and much smaller intercept, which is close to zero. Remarkably, the intercept can be numerically expressed as $\alpha_\pi(0) = -m_\pi^2\alpha'_\pi$. This allows us to parameterize the pion trajectory in terms of the pion mass and the slope parameter:

$$\alpha_{\pi_0}(s) = -\alpha'_\pi(m_\pi^2 - s) \quad \text{with} \quad m_\pi = \sqrt{\frac{|\alpha_\pi|}{\alpha'_\pi}} \approx 0.14\,\mathrm{GeV}\,. \tag{35}$$

However, the *"established"* trajectory (34) is disfavored by the fifth state $\pi_4(2250)$ (a fit within a linear trajectory to all five states provides $\chi^2/\mathrm{d.o.f.} \approx 3.5$). From Fig. 2 it seems to be obvious that the anomalous behavior of the trajectory appears at low J values rather than large ones, see for example curve (dotted) and compare also with master trajectory. If we now adapt the heavy pion world ($m_\pi^2 \sim 600\,\mathrm{MeV}^2$), the π_0/b_1 trajectory (35) could be viewed as linear and parallel to the master one. On the other hand in the chiral limit $m_\pi \to 0$ the pion might be viewed as a singular state that does not belong to a linear b_1/π_2-trajectory, connecting the other four states.

Presumably, the non-linearity of the π_0/b_1-trajectory is related to spontaneous chiral symmetry breaking. However, we believe that the chiral limit does not provide a perfect guidance to model

builders that are interested to describe the real world. Thus, we should in fact utilize a non-linear pion trajectory rather than a pion pole. However, for simplicity we compromise and choose the hypothetic a_1/ρ_2- and π_0/b_1-trajectory to be linear within a common slope parameter that is smaller and larger than those of the *"established"* a_1/ρ_2- and π_0/b_1-trajectory, respectively,

$$\alpha(t) = \alpha + \alpha' t\,, \quad \alpha = \frac{1}{2}\,,\ \alpha' = \frac{4}{5\,\mathrm{GeV}^2}\,; \quad \alpha_\pi(t) = \alpha_\pi + \alpha' t\,, \quad \alpha_\pi = -m_\pi^2 \alpha'\,,\ m_\pi = 0.14\,\mathrm{GeV}\,. \tag{36}$$

Here and in the following we denote a leading master trajectory as $\alpha(t)$ and its intercept with the shorthand

$$\alpha \equiv \alpha(t=0).$$

3.2 Modelling $\widetilde{H}^{(3)}_{jj}$

3.2.1 $t = 0$ case: polarized PDFs

We consider first the $t = 0$ case of the leading SO(3) PW amplitudes in conformal GPD moments. They coincide then with the common Mellin moments of the polarized PDF:

$$\widetilde{H}^{(3)\pm}_{jj}(t=0) \equiv \Delta q^{(3)\pm}_j \quad \text{for} \quad j = \begin{cases} \text{even}\ (+) \\ \text{odd}\ \ (-) \end{cases}\,, \tag{37}$$

cf. Eq. (20). For even and odd j the parity charge-even and -odd type PDFs are to be taken

$$\Delta q^{(3)\pm}_j = \int_0^1 dx\ x^j \Delta q^{(3)\pm}(x)\,, \quad \Delta q^{(3)\pm} = \Delta u - \Delta d \pm \left(\Delta\bar{u} - \Delta\bar{d}\right), \quad j = \begin{cases} \text{even}\ (+) \\ \text{odd}\ \ (-) \end{cases}. \tag{38}$$

We also distinguish between valence, sea, and anti-quarks, where the sea content of polarized quarks is expressed by the anti-quarks $\Delta\bar{q}(x)$. The polarized charge parity-even PDF is then given as sum of valence quarks and antiquarks and the charge parity-odd one is equated to valence quarks[3]:

$$\Delta q^+(x) = \Delta q^{\mathrm{val}}(|x|) + \Delta q^{\mathrm{sea}}(|x|)\,, \quad \Delta q^{\mathrm{sea}}(|x|) = 2\Delta\bar{q}(|x|)\,, \quad \Delta q^-(x) = \mathrm{sign}(x)\,\Delta q^{\mathrm{val}}(|x|)\,. \tag{39}$$

Let us make a side remark with respect to the 'spin puzzle', which we understand as the mismatch of quark model and partonic degrees of freedom. In the quark model the nucleon possesses no antiquarks and its constituents are considered as collective degrees of freedom. Loosely spoken, the constituent quarks are somehow made up from the partonic content. If one literally identifies the partonic and quark model degrees of freedom, one easily generates momentum fraction or spin 'puzzles'. It might be somehow legitimate to identify the collective constituent quarks with the partonic valence quarks [66] and one might wonder whether the 'spin puzzle' exists then. The 'spin

[3] For convenience, we proceed in momentum fraction space and below in Sect. 3.2.2 we return to Mellin space.

puzzle' is perhaps easily solved by an appropriate matching prescription of collective and partonic degrees of freedom or, as in the case of the 'momentum fraction puzzle', one simply accept that one deals with different degrees of freedom. Of course, the decomposition of the proton spin in terms of its fundamental degrees of freedom remains a serious challenge.

Although it is rather likely that SU(6) symmetry in polarized valence quark PDFs holds true at small-x values and it is broken in the large-x region, we find it interesting to explore the valence matching scheme of collective and partonic degrees of freedom. To do so, we adapt flavor-spin SU(6) [SU(3) $\otimes$ SU(2)] symmetry to fix the normalization of polarized valence quarks in the iso-vector sector by the group theoretical value of the axial-vector coupling $g_A^{\rm val}$:

$$\begin{aligned} g_A^{\rm val} \equiv \int_0^1 \Delta q^{(3)-}(x) &= u^{\uparrow,{\rm val}} - u^{\downarrow,{\rm val}} - d^{\uparrow,{\rm val}} + d^{\downarrow,{\rm val}} \\ &\overset{\rm SU(6)}{=} \frac{4}{3} - \frac{-1}{3} = \frac{5}{3}. \end{aligned} \tag{40}$$

The axial-vector charge g_A, i.e., the expectation value of the axial-vector current in the forward kinematics, is given by the lowest moment of the polarized charge parity-even quark PDFs. Hence, both valence and sea quarks contribute:

$$\begin{aligned} g_A \equiv \int_0^1 \Delta q^{(3)+}(x) &= u^{\uparrow,{\rm val}} - u^{\downarrow,{\rm val}} - d^{\uparrow,{\rm val}} + d^{\downarrow,{\rm val}} + 2\left(\overline{u}^{\uparrow} - \overline{u}^{\downarrow} - \overline{d}^{\uparrow} + \overline{d}^{\downarrow}\right) \\ &\overset{\rm exp}{=} 1.2670 \pm 0.0035\,, \end{aligned} \tag{41}$$

and the experimental value, taken from Ref. [51], is smaller than the SU(6) quark model expectation. For an isospin symmetric polarized sea, the axial-vector charge g_A reduces to its valence part $g_A^{\rm val}$. In such an ad hoc scenario, historically used for simplicity, e.g., in standard PDF fits, the SU(6) value (40) contradicts the experimental finding (41). We clearly spell out that the SU(6) value (40) is not ruled out and a 'spin puzzle' does not exist. Rather SU(6) symmetry forces us to introduce an isospin asymmetric sea with a large negative net contribution

$$\begin{aligned} g_A^{\rm sea} \equiv \int_0^1 dx\, \Delta q^{(3){\rm sea}}(x) &= 2\left(\overline{u}^{\uparrow} - \overline{u}^{\downarrow} - \overline{d}^{\uparrow} + \overline{d}^{\downarrow}\right) \\ &\overset{\rm SU(6)}{=} -\frac{2}{5}\,. \end{aligned} \tag{42}$$

Here we used that $g_A = 5/3 - 2/5 \approx 1.267$ is the mean of the experimental value (41). As we will see below, this SU(6) symmetric valence scenario is also not ruled out by polarized DIS measurements and some lattice simulations. Our scenario is in conflict with chiral quark soliton model (χQSM) considerations [67, 68, 69, 70, 71], predicting a flavor asymmetric sea within a positive value for $g_A^{\rm sea}$; however, qualitatively supported by meson cloud model considerations, suggesting a (small) negative value of $g_A^{\rm sea}$ [72, 73, 74, 75].

The next ingredient for our generic PDF model are large-x counting rules, obtained from dimensional counting or diagrammatic analysis [76, 77]. They state that for a proton with helicity $+1/2$ a quark PDF vanishes for $x \to 1$ as $(1-x)^\gamma$, where the power

$$\gamma = 2n_s - 1 + (1 - 2h) \tag{43}$$

is determined by the number of spectators n_s and the helicity $h = \pm 1/2$ of the struck quark [37]. For valence and sea quarks with helicity aligned to the proton one the exponent γ is given by $\beta = 3$ and $\beta = 7$, respectively. If the struck quark helicity is anti-aligned these values increase by $\delta\beta = 2$ to $\beta + \delta\beta$. We recall that the small-x behavior of our polarized PDF is determined by the intercept of the hypothetical master trajectory (33), i.e., $\lim_{x\to 0} \Delta q(x) \propto x^{-\alpha}$, which we set to the generic value (36), $\alpha = 1/2$.

The small and large-x behavior are incorporated in a factorized ansatz:

$$\begin{aligned} \Delta q^{(3)}(x) &\equiv \widetilde{H}^{(3)}(x, \eta = 0, t = 0) \\ &= g_A \, x^{-\alpha} \frac{(1-x)^\beta - \widetilde{h}\,(1-x)^{\beta+\delta\beta}}{B(1-\alpha, 1+\beta) - \widetilde{h}\, B(1-\alpha, 1+\beta+\delta\beta)} \,, \end{aligned} \tag{44}$$

where the normalization of the lowest Mellin moment is given by the corresponding partonic axial-vector couplings $g_A^{\rm val}$ and $g_A^{\rm sea}$. In the partonic model interpretation the $\widetilde{h}$ parameter adjusts the ratio of quarks with aligned and anti-aligned helicities. We might assume that at small-x the sea quark density becomes helicity independent, i.e., we set $\widetilde{h}^{\rm sea} = 1$. For this specific value the polarized PDF (44) behaves with $\alpha = 1/2$ in the small-x region as $x^{1-\alpha} = x^{1/2}$, which is nothing but the Regge behavior that belongs to the established a_1 trajectory, cf. Eq. (31), [78]. However, the partonic interpretation of $\widetilde{h}^{\rm sea}$ might be too rigid for $\widetilde{h}^{\rm val}$. Namely, at large-x also a certain amount of valence quarks with aligned helicities might be suppressed by some additional powers of $(1-x)^{\Delta\beta}$ [37]. We choose $\Delta\beta = \delta\beta = 2$ and consider now $\widetilde{h}^{\rm val}$ as an effective parameter. In the following considerations we set $\widetilde{h}^{\rm val} \stackrel{\rm phe}{=} 0.85$. Relying on our partonic inspiration, the hypothetical Regge intercept, SU(6) symmetric valence scenario, and canonical counting rules, we can fix the model parameters:

$$\begin{aligned} \alpha \stackrel{\rm gen}{=} \frac{1}{2}\,, \quad \alpha' \stackrel{\rm gen}{=} \frac{4}{5}\,, \qquad & g_A^{\rm val} \stackrel{\rm SU(6)}{=} \frac{5}{3}\,, \qquad \widetilde{h}^{\rm val} \stackrel{\rm phe}{=} 0.85\,, \quad \beta^{\rm val} \stackrel{\rm gen}{=} 3\,, \quad \delta^{\rm val}\beta \stackrel{\rm gen}{=} 2\,, \\ & g_A^{\rm sea} \stackrel{\rm SU(6)}{=} -\frac{2}{5}\,, \quad \widetilde{h}^{\rm sea} \stackrel{\rm gen}{=} 1\,, \qquad \beta^{\rm sea} \stackrel{\rm gen}{=} 7\,, \quad \delta^{\rm sea}\beta \stackrel{\rm gen}{=} 2\,, \end{aligned} \tag{45}$$

where also the generic Regge slope parameter, see Eq. (36), is included.

A few comments are in order. For our convenience we take the parameters, specified in (45), at the input scale $\mu^2 = 2\,{\rm GeV}^2$. The phenomenological values for β and $\delta\beta$ should in accordance with evolution be moderately larger while the hypothetical Regge intercept α is rather robust

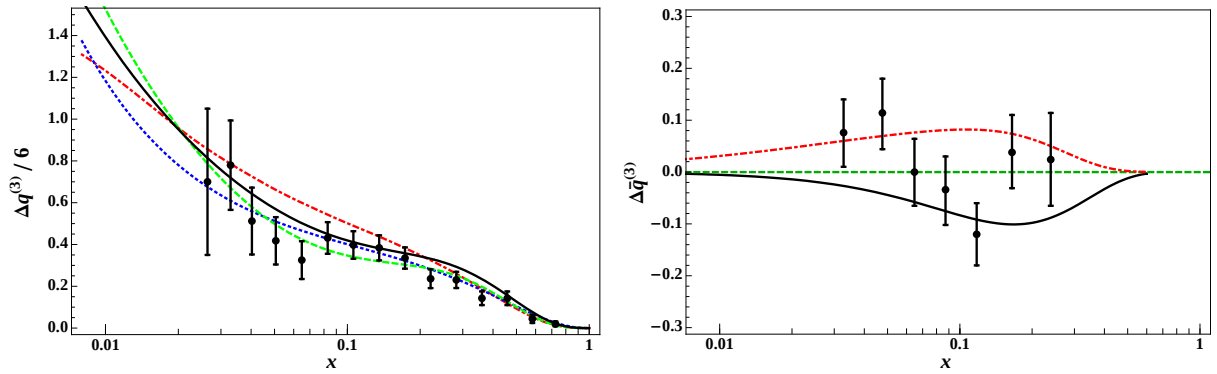

Figure 3: Standard LO PDF parameterizations, described in the text, and a generic PDF model (solid), specified in Eqs. (44) and (45), are confronted with HERMES results [79, 80] for the DIS structure function $g_1^{(3)}(x)$ (left) and $(\Delta\overline{u} - \Delta\overline{d})(x)$ (right), where only statistical errors are shown.

under evolution. Instead of a SU(6) symmetric valence scenario we could also have adopted a standard one from the literature. After an appropriate change of $\widetilde{h}^{\rm val/sea}$, all of these scenarios allow us to describe the measurements, discussed in this article. We add that the model can be easily extended to unpolarized PDFs. In such a framework the parameters $\widetilde{h}^{\rm val/sea}$, considered as effective ones, can be constrained from the large-x behavior of DIS structure functions. It is beyond the scope of this paper to present such studies.

The iso-vector part of the polarized structure function, expressed at LO by the polarized PDF, can be experimentally obtained from DIS measurements on proton and neutron target:

$$\begin{aligned} g_1^{(3)}(x_{\rm B}, \mathcal{Q}^2) &\equiv g_1^{(p)}(x_{\rm B}, \mathcal{Q}^2) - g_1^{(n)}(x_{\rm B}, \mathcal{Q}^2) \\ &\stackrel{\rm LO}{=} \frac{1}{6}\Delta q^{(3)+}(x = x_{\rm B}, \mu^2 = \mathcal{Q}^2)\,. \end{aligned} \tag{46}$$

Here we conventionally set the scale $\mu^2 = \mathcal{Q}^2$. Our generic PDF model fairly agrees with standard polarized PDF parameterizations, taken at the input scale $\mu^2 = 2\,{\rm GeV}^2$. This is illustrated in the left panel of Fig. 3, where our model (solid) is displayed together with measurements of the HERMES collaboration [79], and standard parameterizations: Gehrmann/Stirling A (95) [81] (dashed), Blümlein/Böttcher (02) scenario 1 [82] (dotted), and Glück/Reya/Stratmann/Vogelsang (00) 'broken valence' scenario [83] (dot-dashed). Note that we fixed in all PDF parameterizations $\mathcal{Q}^2 = 2\,{\rm GeV}$ and that the various parameterizations have a rather different partonic interpretation. The GS and BB parameterizations rely on a flavor symmetric polarized sea, the 'broken valence' GRSV scenario possesses a positive sign for the polarized sea in the iso-vector sector, contrarily, to our SU(6) symmetric valence scenario which requires a negative sign. Hence, the valence and sea quark content of the axial-vector charge is rather different, too. Also the small-x behavior of the various parameterizations differ. Since the areas under the PDF curves in the left panel

of Fig. 3 are fixed by the Bjorken sum rule (or equivalently the normalization condition (41) for the axial-vector current), the small-x behavior of the various parameterizations is essentially a consequence of the assumed large-x behavior and the specific parameterization, in particular, the flavor scheme for the polarized sea.

Semi-inclusive pion production allows addressing polarized antiquarks in the iso-vector sector. In the right panel of Fig. 3 we show the partonic interpretation of a HERMES measurement [80], obtained from a LO fit (full circles), together with various PDF parameterizations. The 'measurement' suggests that $x(\Delta\overline{u} - \Delta\overline{d})(x)$ is highly non-symmetric, where its sign might even change in different x regions; however, statistically, the asymmetry is also compatibly with zero. The figure also illustrates that present experimental data do not allow to quantify the polarized sea and that even a qualitative judgement on the different scenarios can not be drawn. This conclusion is based on more solid ground, namely, on the extensive analysis of polarized PDF uncertainties in global fits from Ref. [84]. Our SU(6) symmetric valence scenario is supported by global fits from Ref. [85].

Because of the polarized PDF uncertainties, one might wonder whether the so-called 'spin puzzle' or 'crisis' in the iso-vector sector has ever existed. The variety in the behavior of standard polarized PDF parameterizations might be also rather important for GPD model builders. Namely, these PDF uncertainties might propagate into GPD model predictions for hard exclusive processes.

3.2.2 t-decoration via Regge trajectories

To decorate the conformal GPD moments (37) with t-dependence, we rely on dimensional counting rules for the large $-t$ behavior of form factors. Lattice results clearly show that with increasing j, i.e., in the momentum fraction representation in the limit $x \to 1$, the t-dependence dies out [86, 87]. To unify these features with Regge behavior, we write the t-dependence as product of monopoles, build up from the leading Regge trajectory and its daughters:

$$\widetilde{H}^{(3)}_{jj}(t) = \frac{(1+j-\alpha)_p}{(1+j-\alpha(t))_p}\Delta q^{(3)}_j\,, \quad \alpha(t) \overset{\text{gen}}{=} \frac{1}{2} + \frac{4\,t}{5\,\text{GeV}^2}\,, \tag{47}$$

where the Pochhammer symbol for integral $p > 0$ is defined as

$$(x)_p = x(x+1)\cdots(x+p-1)$$

and the intercept α has the same value as in the polarized PDF (44). Hence, the zeros of the pre-factor in our model (47) cancel the corresponding poles in the PDF moments, which are then replaced by a product of t-dependent Regge poles $1/[1+j-\alpha(t)]\cdots[p+j-\alpha(t)]$. The number p determines the asymptotic of the PW amplitudes (47) at $-t \to \infty$, which behave as $(-t)^{-p}$. Employing the Drell-Yan exclusive-inclusive relation $\gamma = 2p-1$ [88], we should choose $p = 2$ and

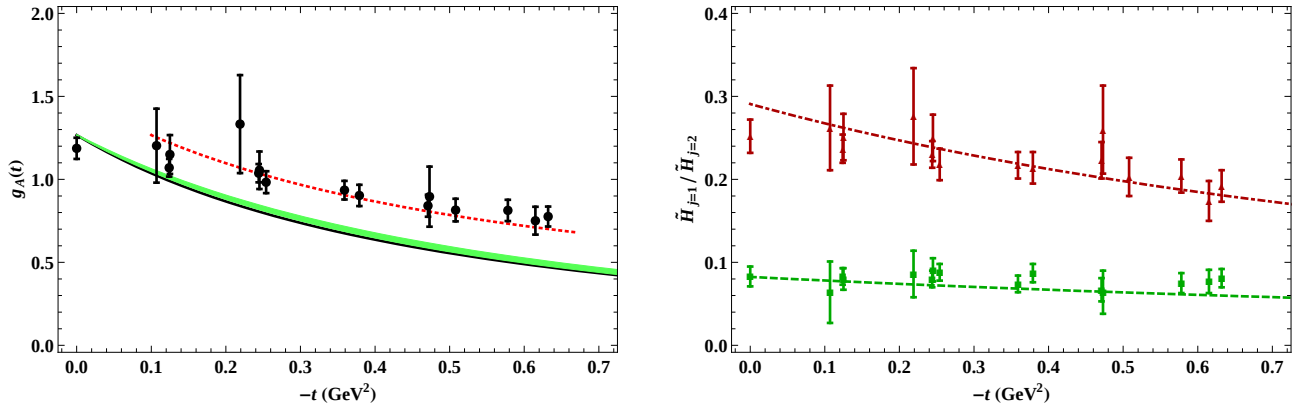

Figure 4: The left panel shows the axial-vector form factor versus $-t$: world fit (48) [error band], generic $\widetilde{H}$ GPD model (47) [solid], as specified in the text, and lattice results (full circles). In the right panel the same GPD model is confronted with lattice data for generalized form factors: $j = 1$ (dot-dashed, triangles) and $j = 2$ (dashed, squares). The scale is $\mu^2 = 4\,\mathrm{GeV}^2$ and lattice measurements are taken from data set VI of Ref. [89].

$p = 4$ for valence ($\gamma = 3$) and sea quarks ($\gamma = 7$), respectively. To simplify the model procedure, we take for both contributions $p = 2$ and we complete the Regge intercept to a generic leading meson trajectory (45).

We illustrate in the left panel of Fig. 4 that the t-dependence of the monopole product ansatz (47) for $j = 0$, displayed as solid curve, is in fair agreement with world dipole fits (error band),

$$g_A(t) = \frac{g_A(0)}{\left(1 - \frac{t}{M_A^2}\right)^2}, \qquad M_A^2 = (1.069 \pm 0.016)\,\mathrm{GeV}^2 \;\left[(1.026 \pm 0.021)\,\mathrm{GeV}^2\right], \tag{48}$$

to the axial-vector form factor measurements from π^+ electroproduction and neutrino scattering experiments [M_A^2 given in square brackets], taken from Ref. [90]. We also display lattice data (full circles) from the set VI of Ref. [89], which at larger $-t$ considerables overshoot the experimental measurements (only statistical errors are shown) and possess at low $-t$ a rather flat t-dependence. The dotted curve is included for illustration and it arises from a shift of our solid model curve. In the right panel of Fig. 4 we plot the second (dot-dashed) and third (dashed) moment (47) versus $-t$ for $\mu^2 = 4\,\mathrm{GeV}^2$, where the polarized PDF moments are specified in Eq. (45) at $\mu^2 = 2\,\mathrm{GeV}^2$. Our generic model predictions are now compatible with lattice data. We emphasize that in particular the lattice result for the $j = 1$ valence generalized form factor at $t = 0$, given as[4] 0.25 ± 0.02, does not "rule out" the SU(6) symmetric valence scenario prediction ≈ 0.29. In standard PDF

[4]Lattice measurements suffer from systematical uncertainties that can hardly be estimated and so it is common to quote only the statistical error.

parameterizations the $j=1$ Mellin moment is typically smaller, namely, ≈ 0.2. Note that this discrepancy in the valence sector essentially originates from the difference between non-standard flavor scheme (45) and flavor symmetric polarized sea.

Finally, we summarize our generic model. Analogous as for PDFs in Eqs. (38) and (39), the odd j (or $-$) moments are entirely associated with valence quarks while the even (or $+$) moments are given by the sum of sea and valence quark contributions. We plug the Mellin moments (38) of our PDF ansatz (44) into Eq. (47) and obtain so the leading SO(3) PW amplitudes

$$\begin{aligned}
&\widetilde{H}^{(3)+}_{jj} = \widetilde{H}^{(3)\rm val}_{jj} + \widetilde{H}^{(3)\rm sea}_{jj}\,, \qquad \widetilde{H}^{(3)-}_{jj} = \widetilde{H}^{(3)\rm val}_{jj}\,, \quad \text{with} \\
&\widetilde{H}^{(3)}_{jj}(t) = g_A\,\frac{(1+j-\alpha)_p}{(1+j-\alpha(t))_p}\,\frac{B(1+j-\alpha,1+\beta)-\widetilde{h}\,B(1+j-\alpha,1+\beta+\delta\beta)}{B(1-\alpha,\beta+1)-\widetilde{h}\,B(1-\alpha,1+\beta+\delta\beta)}\,,
\end{aligned} \tag{49}$$

where the model parameters are specified in Eq. (45).

3.3 Modelling $\widetilde{E}^{(3)}_{jj}$

Analogous as in the previous section, we build now a generic model for the leading SO(3) PW amplitude $\widetilde{E}_{j,J=j}(t)$. Thereby, we borrow us the j-dependence at $t=0$ from the ansatz (49) for $\widetilde{H}_{jj}(t=0)$ with generic Regge intercept $\alpha=1/2$. The new $\{\beta,\delta\beta,\widetilde{e}\}$ parameter set ($\widetilde{h}$ is replaced by $\widetilde{e}$, and to lighten the notation, we use the same symbols β and $\delta\beta$ as for $\widetilde{H}$) will be specified below.

At large $-t$ the helicity non-conserved moments $\widetilde{E}_{jj}(t)$ should decrease by one power of $(-t)^{-1}$ faster than $\widetilde{H}_{jj}(t)$, i.e., it should generically behave as $1/(-t)^3$. In the heavy pion world, in which the π_0/b_1 trajectory is presumably degenerated with the a_1/ρ_2 one, we would write the t-dependence of $\widetilde{E}_{jj}(t)$ as a product of three monopoles,

$$\frac{(j-\alpha_\pi)_3}{(j-\alpha_\pi(t))_3}\,, \quad (\text{where } \; j=J)\,,$$

which are expressed in terms of the π_0/b_1 Regge trajectory and its first two daughters. In the real world we choose the Regge trajectory (35), however, we assume that its two daughters are now degenerated with those of the generic master trajectory $\alpha(t)$. Finally, we introduce the partonic decomposition of even and odd Mellin moments and we write our ansatz for them as follows:

$$\begin{aligned}
&\widetilde{E}^{(3)+}_{jj} = \widetilde{E}^{(3),\rm val}_{jj} + \widetilde{E}^{(3),\rm sea}_{jj}\,, \qquad \widetilde{E}^{(3)-}_{jj} = \widetilde{E}^{(3),\rm val}_{jj}\,, \\
&\widetilde{E}^{(3)}_{jj}(t) = g_P\frac{\alpha'_\pi\,\text{GeV}^2}{j-\alpha_\pi(t)}\,\frac{(1+j-\alpha)_2}{(1+j-\alpha(t))_2}\,\frac{B(1+j-\alpha,1+\beta)-\widetilde{e}\,B(1+j-\alpha,1+\beta+\delta\beta)}{B(1-\alpha,1+\beta)-\widetilde{e}\,B(1-\alpha,1+\beta+\delta\beta)}\,,
\end{aligned} \tag{50}$$

where the generic and pion Regge trajectories are specified in Eq. (36), respectively. Our model for even j is normalized at $j=J=0$,

$$\widetilde{E}^{(3)+}_{00}(t) \equiv g_P(t) = \frac{g_P\,\text{GeV}^2}{m_\pi^2-t}\,\frac{(1-\alpha)_2}{(1-\alpha(t))_2}\,, \quad g_P \equiv g_P^+ = g_P^{\rm val} + g_P^{\rm sea}\,, \tag{51}$$

by the pseudoscalar coupling g_P. In our partonic interpretation it contains a valence and sea quark part, where the former one also determines the normalization of the odd j (or $-$) GPD moments. The lowest moment (51) is nothing but the pseudoscalar nucleon form factor. As designed, our parameterization (51) possesses the pion pole, which appears by means of Eq. (35) as follows:

$$\frac{\alpha'_\pi}{j-\alpha_\pi(t)} \quad \stackrel{j=0}{\Rightarrow} \quad \frac{\alpha'_\pi}{-\alpha_\pi-\alpha'_\pi t}=\frac{1}{m_\pi^2-t} \quad \text{with} \quad m_\pi^2=-\frac{\alpha_\pi}{\alpha'}\,.$$

Let us show that our generic GPD model satisfy the well-known low energy constraints that arise from the hypothesis of a partial conserved axial-vector current (PCAC). PCAC relates the axial-vector and pseudo-scalar form factor, in our notation the GPD combination (26) for $j=0$, with the pion-nucleon form factor:

$$\widetilde{H}^+_{00}(t)+\frac{t}{4M^2}\widetilde{E}^+_{00}(t)=\frac{f_\pi}{\sqrt{2}M}\frac{m_\pi^2}{m_\pi^2-t}G_{\pi NN}(t)\,. \tag{52}$$

For the pion-nucleon form factor we adopt the popular monopole parameterization

$$G_{\pi NN}(t)=\frac{G_{\pi NN}}{1-t/\Lambda^2}\,, \quad G_{\pi NN}\approx 13\,, \;\; \Lambda\approx 0.8\,\text{GeV}\,. \tag{53}$$

In the $t\to 0$ limit ($m_\pi>0$) the Goldberger-Treiman relation shows up, which ties the axial-vector coupling to the pion-nucleon coupling $g_A=f_\pi G_{\pi NN}/\sqrt{2}M$ [91]. In the chiral limit ($m_\pi\to 0$) the axial-current is conserved and the r.h.s. of Eq. (52) vanishes. Our ansaetze (49) and (50) are so designed that the resulting constraint

$$\lim_{m_\pi\to 0}\frac{-t}{4M^2}\widetilde{E}^+_{00}(t)=\widetilde{H}^+_{00}(t) \quad \text{with} \quad g_P=4g_AM^2/\text{GeV}^2 \tag{54}$$

is satisfied within the well-known relation of pseudoscalar and axial-vector coupling. If we now modify the relation between (partonic) pseudoscalar and axial-vector couplings by a small m_π^2 proportional term,

$$g_P^{\text{val/sea}}=g_A^{\text{val/sea}}\frac{2-\alpha+m_\pi^2\alpha'}{2-\alpha}4M^2/\text{GeV}^2\,, \quad g_A\equiv g_A^{\text{val}}+g_A^{\text{sea}}\approx 1.267\,, \tag{55}$$

and set in the pion-nucleon form factor (53) the monopole mass $\Lambda=\sqrt{(1-\alpha)/\alpha'}$, our model exactly satisfies the PCAC relation (52). Moreover, within the generic Regge parameters (36) we find for the monopole mass the phenomenological value that is quoted in Eq. (53). Since we satisfy the PCAC relation and have a realistic description of the axial-vector form factor, see left panel in Fig. 4, we also describe in the left panel of Fig. 5 the t-dependence of the pseudo-scalar form factor (51) measurements.

We specify now the remaining parameter set $\{\beta,\delta\beta,\widetilde{e}\}$ for both valence and sea quarks. As in Sect. 3.2, these parameters could be partly read off from large-x counting rules. Unfortunately, to

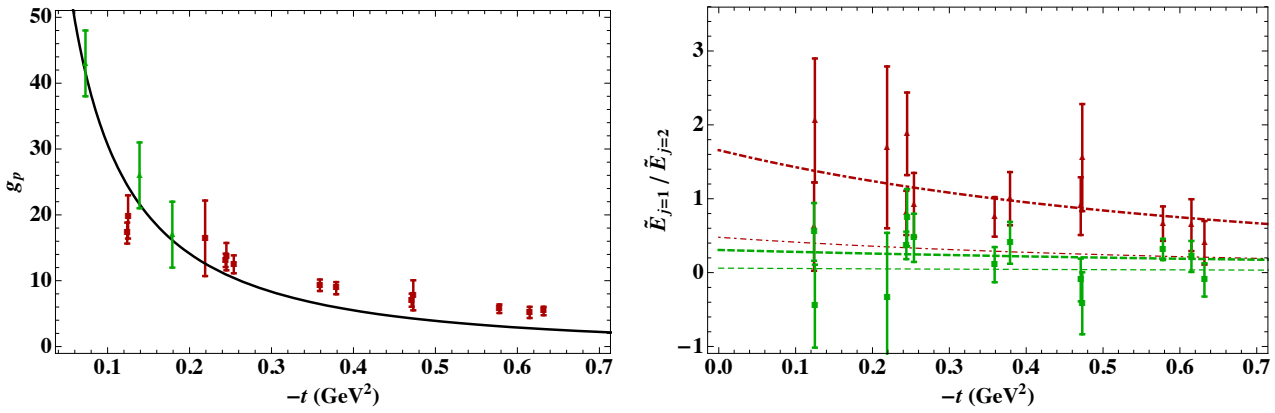

Figure 5: In the left panel the pseudo-scalar form factor is displayed: generic model (50) prediction (solid curve), experimental [92] (triangles) and lattice (squares) data. In the right panel GPD model (50) predictions within parameters (56) [thick] and (57) [thin] and lattice results for generalized form factors are presented: $j = 1$ (dot-dashed, triangles) and $j = 2$ (dashed, squares). Same scale specification and lattice data as in Fig. 4.

our best knowledge, for $\widetilde{E}$ GPD such counting rules are not presented in the literature. We might expect that due to the non-conserved target helicity a $\widetilde{E}$ GPD decreases by two powers of $(1-x)$ faster at large x than a $\widetilde{H}$ GPD. Our $\widetilde{E}$ GPD Mellin moments (50) behave as $j^{-\beta-2}$ for $j \to \infty$ and, thus, in the limit $x \to 1$ the zero-skewness $\widetilde{E}$ GPD vanishes as $(1-x)^{\beta+1}$. For simplicity, we take this relative $(1-x)$ suppression factor in our model, i.e., we take for the $\widetilde{E}$ GPDs the same generic values for β (and also for $\delta\beta$) as for $\widetilde{H}$ GPDs, specified in Eq. (45).

Now the $\widetilde{e}$ parameters can be used to tune the decrease of the $\widetilde{E}$ GPD Mellin moments (50) with growing j. To some extent they might be constrained by lattice data for generalized form factors (set VI of Ref. [89]), shown in the right panel of Fig. 5. We use again our SU(6) symmetric valence scenario (45) within a flavor asymmetric sea and evolve our moments, specified at $\mu^2 = 2\,\mathrm{GeV}^2$, to the scale $\mu^2 = 4\,\mathrm{GeV}^2$ of Ref. [89]. For $j = 1$ we find that $\widetilde{e}^{\,\mathrm{val}}$ is slightly larger than one (triangles, thick dot-dashed curve). Since the $j = 2$ generalized form factor data (squares) are compatible with zero and very noisy, the sea quark parameter $\widetilde{e}^{\,\mathrm{sea}}$ is essentially not constrained by data. We choose the parameter set

$$\widetilde{e}^{\,\mathrm{val}} \overset{\mathrm{Lat}}{=} 1.1\,, \quad \widetilde{e}^{\,\mathrm{sea}} \overset{\mathrm{gen}}{=} 1\,, \tag{56}$$

which is fully compatible with lattice data (thick curves). Below we will also use the set

$$\widetilde{e}^{\,\mathrm{val}} = \widetilde{e}^{\,\mathrm{sea}} = 0\,, \tag{57}$$

which is, however, disfavored by the lattice measurement of the $j = 1$ generalized form factor, see thin dot-dashed curve.

Finally, we summarize our $\widetilde{E}_{jj}$ GPD model. It arises from plugging the PCAC relation (55) into the ansatz (50):

$$\widetilde{E}^{(3)+}_{jj} = \widetilde{E}^{(3),\text{val}}_{jj} + \widetilde{E}^{(3),\text{sea}}_{jj}\,, \qquad \widetilde{E}^{(3)-}_{jj} = \widetilde{E}^{(3),\text{val}}_{jj}\,, \quad \text{with} \tag{58}$$
$$\widetilde{E}^{(3)}_{jj}(t) = \frac{4g_A\alpha' M^2(2-\alpha-\alpha_\pi)\,(1+j-\alpha)_2}{(2-\alpha)(j-\alpha_\pi(t))\,(1+j-\alpha(t))_2}\frac{B(1+j-\alpha,1+\beta)-\widetilde{e}\,B(1+j-\alpha,1+\beta+\delta\beta)}{B(1-\alpha,1+\beta)-\widetilde{e}\,B(1-\alpha,1+\beta+\delta\beta)}\,,$$

the SU(6) symmetric valence scenario, cf. Eq. (45), generic Regge trajectories (36), and by the $\widetilde{e}$ parameters (56) or, alternatively, (57).

3.4 The properties of a minimalist GPD model

Let us shortly recall that at LO accuracy and for (nearly) fixed photon virtuality $\mathcal{Q}^2$ the GPD on the cross-over line $\eta = x$ entirely determines the 'CFFs' [9], see also Ref. [29] for a phenomenological discussion to reveal this GPD from experimental measurements. From Eq. (13) it follows that the imaginary part

$$\Im\text{m}\left\{\begin{matrix}\widetilde{\mathcal{H}}\\ \widetilde{\mathcal{E}}\end{matrix}\right\}(\xi,t,\mathcal{Q}^2) \overset{\text{LO}}{=} \pi\left\{\begin{matrix}\widetilde{H}\\ \widetilde{E}\end{matrix}\right\}(x=\xi,\eta=\xi,t,\mathcal{Q}^2) \tag{59}$$

of a 'CFF' is directly expressed by the GPD on the cross-over line. Moreover, for any GPD, i.e., this function has a double distribution representation, the unsubtracted 'dispersion relations'

$$\Re\text{e}\left\{\begin{matrix}\widetilde{\mathcal{H}}^+\\ \widetilde{\mathcal{E}}^+\end{matrix}\right\}(\xi,t,\mathcal{Q}^2) \overset{\text{LO}}{=} \text{PV}\int_0^1 dx\,\frac{2\xi}{\xi^2-x^2}\left\{\begin{matrix}\widetilde{H}^+\\ \widetilde{E}^+\end{matrix}\right\}(x,\eta=x,t,\mathcal{Q}^2)\,, \tag{60}$$

$$\Re\text{e}\left\{\begin{matrix}\widetilde{\mathcal{H}}^-\\ \widetilde{\mathcal{E}}^-\end{matrix}\right\}(\xi,t,\mathcal{Q}^2) \overset{\text{LO}}{=} \text{PV}\int_0^1 dx\,\frac{2x}{\xi^2-x^2}\left\{\begin{matrix}\widetilde{H}^-\\ \widetilde{E}^-\end{matrix}\right\}(x,\eta=x,t,\mathcal{Q}^2)\,, \tag{61}$$

offer an alternative way to evaluate the real part of CFFs from the GPDs on the cross-over line. To spell it out clearly, these 'dispersion relations' arise from the physical ones in the leading twist-two approximation, i.e., the spectral function and its support $|\xi| \leq \xi_{\text{cut/pol}} = 1$ change [45], and they are in one-to-one correspondence with the LO approximation of CFFs (13).

Only the skewness dependence of the GPD on the cross-over line is relevant for the LO description of experimental data. To quantify this dependence, we define the r-ratio

$$r(x,t,\mathcal{Q}^2|F) = \frac{F(x,\eta=x,t,\mathcal{Q}^2)}{F(x,\eta=0,t,\mathcal{Q}^2)}\,, \qquad F=\{\widetilde{H},\widetilde{E}\} \tag{62}$$

of the GPD on the cross-over line and on the line $\eta = 0$. If this ratio is one, we call it zero skewness effect. Note that the r-ratio is in a LO interpretation of DIS and hard exclusive electroproduction to some extent 'measurable' for H and $\widetilde{H}$ type GPDs.

To build a model for the full $\widetilde{H}^{(3)\pm}$ and $\widetilde{E}^{(3)\pm}$ GPDs, we relate them by a 'holographic principle' to their forward analog. In the following we prefer simplicity and take the *minimalist* 'holographic principle' in conformal Mellin space, see explanations in Ref. [49]. Namely, we equate the conformal GPD moments

$$\widetilde{H}_j(\eta,t) = \widetilde{H}_{jj}(t)\, \hat{d}^{j+1}_{0,1}(\eta) \quad \text{and} \quad \widetilde{E}_j(\eta,t) = \widetilde{E}_{jj}(t)\, \hat{d}^{j}_{0,0}(\eta)\,, \tag{63}$$

with the leading SO(3) PWs $J = j+1$ and $J = j$, specified in Eqs. (22) and (23), respectively. The price of simplicity is that the GPD on the cross-over line is rigid. Our leading SO(3)-PW model (63) can be equivalently set up in a minimalist "dual" parameterization or the Shuvaev transform [93] (where we understand that this name already implies the necessary restriction of the GPD transform [94]). The corresponding GPD and the double distribution have so far not been analytically evaluated, for other model examples see [44, 95]. Numerically, the GPD can be evaluated within a Mellin Barnes integral [44].

We are here only interested on the phenomenological GPD aspect and need only the GPD on the cross-over line. Our specific model assumptions imply a characteristic small-x and large-x behavior, which can be read off from the imaginary part of the Mellin-Barnes integral (21) by means of Eq. (59), where we set $\xi = x$. In the following we are not concerned about evolution and set $\mathcal{Q}^2 = \mathcal{Q}_0^2$ in Eq. (21).

The small-x behavior is determined by the leading Regge pole, which can be picked up by a shift of the integration path to the left hand side. One easily finds a partial factorization of t-dependence and a specific value for the r-ratio [94],

$$\lim_{x\to 0} r(x,t|\widetilde{H}) = \frac{2^{\alpha(t)}\Gamma(3/2+\alpha(t))}{\Gamma(3/2)\Gamma(2+\alpha(t))}\,, \quad \lim_{x\to 0} r(x,t|\widetilde{E}) = \frac{2^{1+\alpha_\pi(t)}\Gamma(5/2+\alpha_\pi(t))}{\Gamma(3/2)\Gamma(3+\alpha_\pi(t))}\,. \tag{64}$$

Since this is nothing but the Clebsch-Gordan coefficient in the conformal PW expansion (21), we call it for $t = 0$ conformal ratio[5] [49]. This ratio is only a function of the leading trajectory $\alpha(t)$ and it is valid for a restricted $\alpha(t)$ interval, i.e., $-t$ is restricted by an upper bound. For $\alpha(t) > 0$ and $\alpha_\pi(t) > -1$ our models possess a positive skewness effect $r > 1$.

The large-x behavior of a minimalist GPD on the cross-over line, can be derived from the large-j behavior of the Mellin-Barnes integrand (21) taken at large x. It arises from the Clebsch-Gordon coefficient, the skewness-zero GPD moments, and the behavior of SO(3) partial waves

$$\hat{d}^{j+\lambda}_{0,\lambda}(x) \sim \frac{\Gamma(3/2)\Gamma(3+j)}{\Gamma(5/2+j)}(x/2)^{j+1}\, 2^{2-3\lambda}(3+2j)^{\lambda}\, e^{j\sqrt{1-x^2}} \quad \text{with} \quad \lambda = \{0,1\}.$$

[5]The name is also motivated by the fact that a minimalist GPD model with leading Regge behavior in the small x-region and for $t = 0$ is equivalent to a conformal GPD model. Since effective Regge behavior is commonly present in a realistic GPD model, we name the ratio for shortness conformal.

Here we utilized the definitions (22) and (23) in terms of hypergeometric functions and their large j asymptotic for $x \to 1$ [96]. Combining all together, and considering the Mellin-Barnes integral as a Fourier transform with conjugate variable $\sqrt{1-x^2} \sim \sqrt{2}\sqrt{1-x}$, we find that our minimalist GPDs behave at $x \to 1$ as

$$\begin{aligned} \widetilde{H}(x,x,t) &\sim (1-x)^{\frac{\beta-1}{2}} \quad \overset{\beta=3}{\Rightarrow} \quad \sim (1-x)^1 \,, \\ \widetilde{E}(x,x,t) &\sim (1-x)^{\frac{\beta+1}{2}} \quad \overset{\beta=3}{\Rightarrow} \quad \sim (1-x)^2 \,. \end{aligned} \tag{65}$$

As required, our findings are consistent with the large-x result in the 'dual' model[6] [97]. The behavior (65) also coincides with the large-x counting as it has been derived for the H and E GPDs from diagrammatic considerations [99]. Hence, compared to the zero-skewness GPD, our GPDs at the cross-over line possess a large enhancement effect. We also note that in our models within linear Regge trajectories the t-dependence dies out at large x with $\sqrt{1-x}$. For fixed t the skewness ratio in the large x-region can be written as

$$\lim_{x\to 1} r(x,t|F) \sim (1-x)^{-\frac{\beta+1}{2}} \frac{F^{\rm red}(\sqrt{2}\sqrt{1-x}\,t)}{F^{\rm red}((1-x)t)} \,, \tag{66}$$

where $F^{\rm red}$ is a reduced GPD that encodes the t-dependence for both $\eta = 0$ and $\eta = x$ cases. From the point of view of light-cone wave function modelling, [100, 101], double distribution models [102, 103, 104], and diagrammatical counting rules [99] one expects that the t-dependence dies out faster for $x \to 1$. It is here far beyond the scope to fix the presumable unrealistic feature in our models, e.g., by employing slightly non-linear Regge trajectories.

For $t = 0$ we illustrate the skewness effect in Fig. 6, where we show GPDs on the lines $\eta = x$ and $\eta = 0$ as thick and thin curves, respectively. More specifically, we plot the dominant charge parity-even GPD models $\widetilde{H}^{(3)+}$ (left) and $x\widetilde{E}^{(3)+}$ (right), where the latter is rescaled by x. Thereby, the $\widetilde{H}$ (49) and $\widetilde{E}$ (58) GPDs are specified by the parameter sets (45) and (56), shown as dot-dot-dashed curve, and alternatively for the $\widetilde{E}$ GPD within the parameters (57) as dot-dashed curves. As one realizes in the right panel the $\widetilde{E}$ GPD models are qualitatively different, however, they approach each other in the small x-region. The characteristic small-x enhancement of a minimalist GPD is controlled by the conformal ratio (64). For our $\widetilde{H}$ and $\widetilde{E}$ GPDs it is given by $r \approx 1.2$ and $r \approx 1.5$, respectively. The large-x enhancement (65) is clearly a big effect for the dot-dot-dashed models. We also observe that, compared to its forward analog, our minimalist GPDs on the cross-over line are enhanced in the valence region. Note that our $\widetilde{E}$ GPD on the cross-over line is always positive, while in the χQSM estimate it can be even negative [105].

[6]For H GPD one might utilize the SO(3)-PWs $d^J_{0,0}$ and so the power is $\beta/2$ in agreement with Ref. [97, 95]. Within SO(3)-PWs $d^J_{0,1}$ polynomiality is not completed and we obtain $(\beta-1)/2 = 1$ for $\beta = 3$, which is consistent with the large x-behavior in Radyushkin's double distribution ansatz with $b = 1$[98].

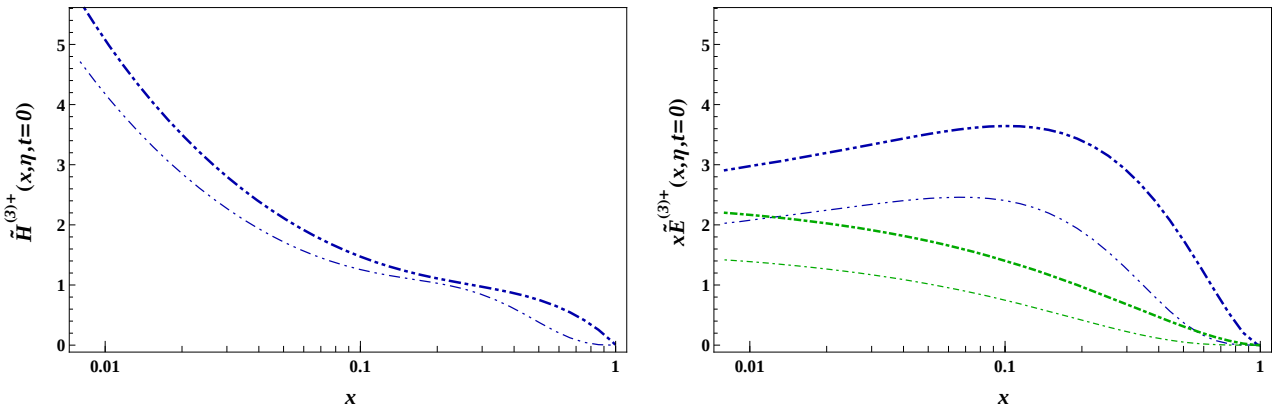

Figure 6: The charge parity-even $\widetilde{H}^{(3)+}(x,x,t=0)$ GPD (left) and scaled $x\widetilde{E}^{(3)+}(x,x,t=0)$ GPD (right) with parameter sets (45) and (57) are shown as dot-dot-dashed curves and for parameters (56) as dot-dashed. The corresponding GPDs at $\eta=0$ are displayed as thin curves.

Let us now point out the particularities of the charge parity-even $\widetilde{E}^{(3)+}$ GPD. This GPD steeply rises as $x^{-1-\alpha_\pi(t)}$ with decreasing x, see the flat behavior of the scaled $x\widetilde{E}$ GPD in the right panel of Fig. 6. Since the small intercept $\alpha_\pi = -m_\pi^2\alpha'$ is negative, it is guaranteed that for $t\leq 0$ the lowest Mellin moment of this GPD exists and that an unsubtracted dispersion relation (60) is sufficient. Because of this singular behavior at $x=0$, the charge parity-even 'CFF' (60) possesses a large real part that can be loosely viewed as a $1/\xi$ proportional constant. To isolate this term, we introduce an over subtraction in the dispersion relation (60) at the point $\xi=\infty$:

$$\Re\mathrm{e}\widetilde{\mathcal{E}}^{(3)+}(\xi,t) \overset{\mathrm{LO}}{=} \frac{1}{\xi}\mathrm{PV}\int_0^1 dx\,\frac{2x^2}{\xi^2-x^2}\widetilde{E}^{(3)+}(x,x,t) + \frac{1}{\xi}C_{\mathcal{E}}(t)\,,\quad C_{\mathcal{E}}(t) = 2\int_0^1 dx\,\widetilde{\mathcal{E}}^{(3)+}(x,x,t)\,. \tag{67}$$

The subtraction constant in this new 'dispersion relation' is evaluated from the GPD on the cross-over line and, thus, it encodes the skewness effect. In the vicinity of $t=m_\pi^2$, we find by means of the Mellin-Barnes integral (21) the pion pole:

$$C_{\mathcal{E}}^{\mathrm{Min}}(t) \overset{\mathrm{LO}}{=} \frac{3}{2}\frac{g_P}{m_\pi^2-t} + \text{non pion-pole contributions}\,. \tag{68}$$

This is nothing but the result in the parameterization of Ref. [14, 16],

$$\widetilde{\mathcal{E}}^{+}_{\pi-\mathrm{pole}}(\xi,t) = \frac{1}{\xi}C^{\mathrm{Min}}_{\pi-\mathrm{pole}}(t)\,,\quad C^{\mathrm{Min}}_{\pi-\mathrm{pole}}(t) = \int_{-1}^1 dx\,\frac{1}{\xi-x}\frac{g_P}{m_\pi^2-t}\frac{\theta(|x|\leq\xi)}{2\,f_\pi}\,\phi_\pi^{\mathrm{asy}}\left(\frac{\xi-x}{2\xi}\right)\,, \tag{69}$$

where the residue is provided by the *asymptotic* pion DA

$$\phi_\pi^{\mathrm{asy}}(u) = f_\pi 6u(1-u). \tag{70}$$

Few comments are in order, which are partially adopted from discussions of parity-even GPDs and the so-called D-term [106] in Refs. [45, 29]:

i. In the parameterization of Ref. [14, 16] the pion-pole lives only in the central GPD region and it is decoupled from the smooth GPD part. This might be the natural answer that arises from a dynamical model calculation, in particular, if the chiral limit is taken. In such a model the cross talk of imaginary and real part is interrupted. On the other hand we can consider the chiral limit of the subtracted dispersion relation (67). Although the intercept is now $\alpha_\pi = -1$, the integral still exists for $t < 0$ and for $t \geq 0$ the answer can be obtained by an analytic regularization of the integral.

ii. One might also reverse the logic, and utilize the subtraction constant (67) as a sum rule that constraints the GPD on the cross-over line.

iii. The residue of the pion pole in the minimalist GPD model, see Eq. (68), is equal to that one in Eq. (69), obtained from the asymptotic DA. This is *not* accidental and it can be viewed from a more general perspective, reflecting the crossing relation between t- and s-channel. Namely, a family of asymptotic generalized DAs, labelled by the t-channel angular momentum J is the crossing analog of the minimalist GPD.

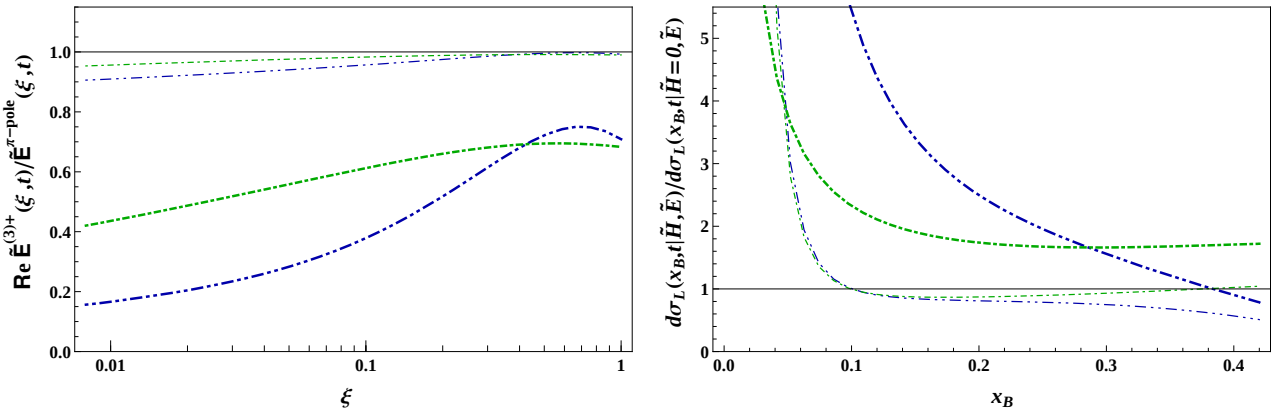

Figure 7: Left panel: $\Re\mathrm{e}\widetilde{\mathcal{E}}^{+}(\xi,t)/\widetilde{\mathcal{E}}^{+}_{\pi-\mathrm{pole}}(\xi,t)$ ratio, cf. Eq. (69), versus ξ for fixed $t = 0$ (thin) and $t = -0.2\,\mathrm{GeV}^2$ (thick). Right panel: cross section ratio $d\sigma_L(x_\mathrm{B}, t'|\widetilde{H}, \widetilde{E})/d\sigma_L(x_\mathrm{B}, t'|\widetilde{H} \equiv 0, \widetilde{E})$ versus x_B for $t' = 0$ (thin) and $t' = -0.2\,\mathrm{GeV}^2$ (thick) with $\mathcal{Q}^2 = 2\,\mathrm{GeV}^2$. The dot-dot-dashed and dot-dashed curves refer to the parameterizations (56) and (57), respectively.

In Fig. 7 we illustrate the role of the pion pole contribution for GPD modelling. In the left panel we show the ratio of the real part of our 'CFF' model to that one of Ref. [15], entirely given by the pion pole contribution (69), versus ξ. For $t = 0$ the ratio is shown as thin curves and as expected it is about one. It slightly gets smaller with decreasing ξ, where the comparison of the dot-dot-dashed (56) and dot-dashed (57) curves reveals that the parameterization of the GPD on the cross-over line has some influence. For non-vanishing $-t$ the difference is more pronounced. Since we neglected the residual t-dependence in the pion pole (69), the ratio considerably decreases

for $-t = 0.2\,\mathrm{GeV}^2$ (thick curves). In the right panel we display the ratio of the unpolarized cross sections (3) for the full $\widetilde{H}$ and $\widetilde{E}$ GPD model (49,58) to that one in which $\widetilde{H}$ is neglected. Thereby, we set $t = t_{\rm min} + t'$. Clearly, only for $t' = 0$ and in some limited $x_{\rm B}$ interval this ratio is around one and so the $\widetilde{E}$ dominance is justified. We conclude that in general kinematics, even in the valence quark region for smaller values of $-t'$, the hard exclusive π^+ electroproduction cross section might *not* be dominated by the pion pole (69).

4 Measurements versus formalism and minimalist model

We like now to confront our minimalist GPD models with the exclusive π^+ electroproduction cross section [30] and single transverse proton spin asymmetry [36] measurements from the HERMES collaboration and the longitudinal photoproduction cross section, measured in Hall C at JLAB, [31, 32]. However, first we will define the observables that can be related to the collinear factorization approach. We like then to comment on the theoretical problems of the collinear factorization approach and we suggest a simple prescription to cure its LO approximation. We finally rely on this prescription and compare our ad hoc GPD models and a tuned one with experimental data.

It is common to convert the electroproduction cross section to the virtual photoproduction one by means of the Hand convention for the photon flux factor Γ_V:

$$\frac{d\sigma^{\gamma^* p\to n\pi^+}}{dt} = \frac{1}{\Gamma_V(x_{\rm B},\mathcal{Q})}\int_0^{2\pi} d\varphi\,\frac{d\sigma^{\pi^+}}{d\mathcal{Q}^2 dx_{\rm B} dt d\phi}\,,\quad \Gamma_V = \frac{\alpha_{\rm em}}{2\pi}\frac{y^2}{1-\varepsilon}\frac{1-x_{\rm B}}{x_{\rm B}\mathcal{Q}^2}\,. \tag{71}$$

The photoproduction cross section can be separated in the transverse and longitudinal part

$$\frac{d\sigma^{\gamma^* p\to n\pi^+}}{dt} = \frac{d\sigma_T^{\gamma^* p\to n\pi^+}}{dt} + \varepsilon\frac{d\sigma_L^{\gamma^* p\to n\pi^+}}{dt}\,. \tag{72}$$

Utilizing the Hand convention (71), we can read off the perturbative prediction for the longitudinal polarized photoproduction cross section from Eq. (3):

$$\frac{d\sigma_L^{\gamma^* p\to n\pi^+}}{dt} \overset{\rm Tw-2}{=} \frac{4\pi^2\alpha_{\rm em}}{\sqrt{1+\epsilon^2}\mathcal{Q}^6}\frac{x_{\rm B}^2}{1-x_{\rm B}}\left\{(1-\xi^2)|\widetilde{\rm H}_{\pi^+}|^2 - \frac{t}{4M^2}|\xi\widetilde{\rm E}_{\pi^+}|^2 - 2\xi^2\Re{\rm e}\,\widetilde{\rm H}_{\pi^+}\widetilde{\rm E}^*_{\pi^+}\right\}\Bigg|_{\xi\to\frac{x_{\rm B}}{2-x_{\rm B}}}\,. \tag{73}$$

If the extraction of the longitudinal photoproduction cross section is experimentally not reachable, a comparison of GPD model predictions for the longitudinal cross section (73) and electroproduction cross section measurements requires a quantitative understanding of its transverse part, too. Utilizing the R ratio, we might express the measured differential photoproduction cross section (71) to its longitudinal part (73) as follows:

$$\frac{d\sigma^{\gamma^* p\to n\pi^+}}{dt} = \left[1+\frac{1}{\varepsilon(x_{\rm B},\mathcal{Q}^2)R(x_{\rm B},t,\mathcal{Q}^2)}\right]\varepsilon(x_{\rm B},\mathcal{Q}^2)\frac{d\sigma_L^{\gamma^* p\to n\pi^+}}{dt}\,,\quad R = \frac{d\sigma_L^{\gamma^* p\to n\pi^+}}{d\sigma_T^{\gamma^* p\to n\pi^+}}\,. \tag{74}$$

Note that the factorization theorem [1] tells us only that the inverse ratio $1/R$ formally vanishes with $1/\mathcal{Q}^2$, however, it does not state that it is numerically small at accessible photon virtualities. Rather it should be expected that $1/R$ is numerically enhanced by non-factorizable contributions, which might also include rather large logarithmical modification of its expected $1/\mathcal{Q}^2$ fall-off; for an example see the perturbative study to the proton Pauli form factor in Ref. [107]. Indeed, measurements in Hall C at JLAB reveal that $1/R$ is rather sizeable for $\mathcal{Q}^2 < 4\,\mathrm{GeV}^2$ and $W \approx 2\,\mathrm{GeV}$ [31, 32].

Unfortunately, to our best knowledge, also a model understanding of the $1/R$ ratio is at present not fully reached. For instance, the Regge-inspired model [33] describes at such low W the longitudinal and the real transverse photoproduction cross section measurements, however, underestimates the virtual transverse one. On the other hand it is in fair agreement with the HERMES measurements for the virtual photoproduction cross section [30]. A refined version of this model, tuned to low energy data from JLAB [34], does describe most of HERMES data, too, however not those at large photon virtualities and relative low energy [35]. In the models the pion pole is reggeized and it essentially contributes only to the longitudinal cross section, which for $|t'| \leq 0.5\,\mathrm{GeV}^2$ is dominant. Hence, for smaller $-t'$ values both models suggest that we can set $1/R$ to zero.

Only the $\sin(\phi - \phi_S)$ harmonic of the single transverse proton spin asymmetry

$$\frac{d^\uparrow\sigma - d^\downarrow\sigma}{d^\uparrow\sigma + d^\downarrow\sigma} = A_{\mathrm{UT}}^{\sin(\phi-\phi_S)} \sin(\phi - \phi_S) + \text{other harmonics}\,, \tag{75}$$

is counted as a further twist-two observable [16], while other harmonics are at least formally suppressed by $1/\mathcal{Q}$. In the notation of Ref. [108] the asymmetry is written in terms of so-called polarized photoabsorption cross sections σ_{mn}^{ij}:

$$A_{\mathrm{UT}}^{\sin(\phi-\phi_S)} = -\frac{\Im\mathrm{m}\left(\boldsymbol{\varepsilon}\,\sigma_{00}^{+-} + \sigma_{++}^{+-}\right)}{\boldsymbol{\varepsilon}\,\sigma_{00}^{++} + \frac{1}{2}\left(\sigma_{++}^{++} + \sigma_{++}^{--}\right)}\,, \tag{76}$$

where the subscripts (superscripts) refer to the photon (target) helicity. Both terms σ_{++}^{+-} and $\sigma_{++}^{++} + \sigma_{++}^{--} \propto d\sigma_T$ arise from the exchange of a transverse polarized photon and, thus, are counted as $1/\mathcal{Q}^2$ power suppressed non-factorizable contributions. We neglect both of them and from the longitudinal cross section (3) we read off the twist-two approximation for the asymmetry

$$A_{\mathrm{UT}}^{\sin(\phi-\phi_S)} \overset{\mathrm{Tw-2}}{=} \left.\frac{-2\sqrt{\frac{t-t_{\min}}{t_{\min}}}\,\xi^2\;\Im\mathrm{m}\,\widetilde{\mathrm{H}}_{\pi^+}\widetilde{\mathrm{E}}_{\pi^+}^*}{(1-\xi^2)|\widetilde{\mathrm{H}}_{\pi^+}|^2 - \frac{t}{4M^2}|\xi\widetilde{\mathrm{E}}_{\pi^+}|^2 - 2\xi^2\Re\mathrm{e}\,\widetilde{\mathrm{H}}_{\pi^+}\widetilde{\mathrm{E}}_{\pi^+}^*}\right|_{\xi\to\frac{x_{\mathrm{B}}}{2-x_{\mathrm{B}}}}\,. \tag{77}$$

Note that the authors of Ref. [16] argued that non-perturbative contaminations mostly cancel in this asymmetry and that a cancellation of perturbative corrections has been numerically established within some GPD models in Refs. [18, 25].

As discussed in Sect. 1, it is an intricate task to judge on the collinear factorization approach, applied to the hard exclusive meson electroproduction. We recall that the hard amplitude is rather analogous as for the pion form factor, where the momentum fractions of the incoming minimal pion Fock state are replaced by those of the emitted and absorbed quarks [18], see Fig. 1b. Moreover, the pion pole plays an important role at very small $-t$ and not too small $x_{\rm B}$. Thus, the theoretical descriptions of the hard exclusive π^+ electroproduction and pion form factor have similarities. The perturbative framework for the pion form factor has been widely discussed in the literature, for critics see Ref. [109, 110], and various improvements were suggested. One might use these recipes to improve the description of hard exclusive meson electroproduction, too, e.g., going back to the overlap representation of Drell and Yan in which the meson wave functions contains transverse degrees of freedom [88], modifying the factorization by incorporating the Sudakov suppression [111, 112], or a scale setting prescription that reshuffles perturbative corrections to the non-perturbative region of the coupling [113].

A popular GPD code is called VGG plus "power corrections". Here the "power corrections" result from a 'hand-bag' calculation in which transverse degrees of freedom (and only the pion pole in the $\widetilde{E}$ GPD) are taken into account [15]. It should be clear from the very beginning that these "power corrections" can not be considered as autonomous contributions and that their interplay with higher Fock state components or so-called soft contributions is not obvious; see also for illustration the light-cone sum rule analysis in Ref. [114]. In some sense this recipe is analog to the Drell-Yan formula for the pion form factor and here the conceptual problem of such an approach is obvious. Namely, the Drell-Yan formula is the starting point and integrating out the transverse degrees of freedom yields the collinear factorization approach. This procedure generates perturbative corrections in the leading twist-two sector [5] and also power suppressed contributions. Strictly spoken, even perturbative and power suppressed contributions can not be autonomously considered as they have a cross talk. Already, for some time it was observed that the sign and magnitude of "power corrections" [15] and perturbative NLO corrections in both DVCS [115, 45] and hard exclusive meson electroproduction [18] match. Although this observation is not quantitatively understood, it reveals the problem of double counting. Hence, one can not take the notion VGG plus "power corrections" literally.

It would be of immense phenomenological interest to estimate the size of perturbative and non-perturbative corrections to the LO formulae (6), (8) of the collinear factorization approach. Since not much is known about power suppressed corrections, we will here assume that they can be neglected. The biggest portion of the large perturbative NLO corrections is proportional to the first coefficient of the $\beta(\alpha_s)$ function [18], which governs the scale change of the running coupling (9). These large corrections can be viewed as an indication for a break down of perturbation

theory. This calls for a resummation procedure, which naturally induces its own ambiguity. Since the LO approximation of the hard scattering amplitude (8) is proportional to the running coupling, a big portion of the NLO corrections can be absorbed by changing the renormalization scale μ_R. The ambiguity we fix by the Brodsky-Lepage-Mackenzie (BLM) scale setting prescription [116] (for the treatment of complex amplitudes see Ref. [117]), yielding

$$\alpha_s\left(\mu_R^{\rm BLM} = \exp\{-f(\xi)/2\}\mathcal{Q}\right) \quad \text{with} \quad e^{-f(\xi)} \lesssim 0.1\,.$$

The resulting renormalization scale, i.e., the function $f(\xi)$, depends on the GPD itself, however, it will be certainly driven into the infrared region and so the coupling itself is now plugged by non-perturbative physics.

The BLM scale in hard exclusive electroproduction is rather small [18, 118], similar as in the perturbative description of the pion form factor [113, 119]. In the following we do not aim for an "optimal" description of the hard exclusive π^+ production rather for a semi-quantitative understanding. Therefore, we simply assume that the effective couplings, arising from the BLM scale setting procedure and the freezing in the infrared region, have in both processes the same value. Hence, within a very low renormalization scale we can employ the LO approximation for the (scaled) pion form factor,

$$\mathcal{Q}^2 F_\pi(\mathcal{Q}^2) \stackrel{\rm LO}{=} 8\pi\alpha_s^{\rm eff} f_\pi^2\, \mathcal{I}_\pi^2(\mathcal{Q}^2)\,, \tag{78}$$

to find the value of this effective coupling. As mentioned, the inverse moment $\mathcal{I}_\pi$, defined in Eq. (10), can be directly revealed at LO from the photon-to-pion transition form factor. Its value, determined from CLEO data [120], would be slightly smaller than one, see, e.g., Refs. [121, 122] for comprehensive discussions. We set it here generically to one, i.e., $\mathcal{I}_\pi(\mathcal{Q}^2) = 1$. This value also arises from the asymptotic pion DA (70) however, also pion DAs with a more complex shape might approximately possess the same value [123, 124, 122]. For the $\mathcal{Q}^2$ scaled pion form factor (78) we take the value 0.36, which is for $\mathcal{Q}^2 > 1.5\,\text{GeV}^2$ and within 1-σ standard deviation compatible with the model dependent extraction of the form factor from the π^+ electroproduction [125], and so we obtain the following value for the effective coupling:

$$\alpha_s^{\rm eff} = 0.8\,. \tag{79}$$

Both the photon-to-pion transition and the elastic pion form factors are described at LO. Note that also within the BLM setting prescription sizeable NLO corrections, related to the Sudakov suppression, affect the LO description of the pion form factor [113].

To provide predictions from our minimalist GPD models, we rely now on the LO approximation of the TFFs (15), where the effective coupling is specified in Eq. (79). Thereby, we employ the

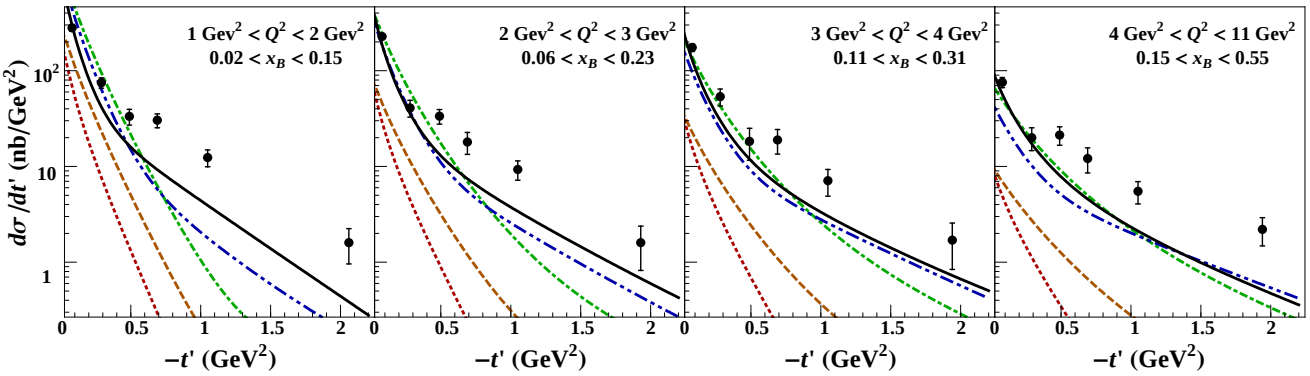

Figure 8: HERMES measurements [30] of the differential cross section $d\sigma^{\gamma^* p\to n\pi^+}/dt'$ versus minimalist GPD model predictions: only with pion pole contribution (dotted), including $\widetilde{H}$ (dashed), full model with the setting (57) and frozen coupling (dot-dashed), same as dot-dashed within parameters (56) (dot-dot-dashed), and versus a tuned GPD model (80) (solid).

Mellin-Barnes integral (21) and the forward Mellin moments (63), which are skewed by the PW amplitudes (49) and (58). We like to add that the integration contour must be chosen carefully and that the dispersion relations (60) and (61) served us to check our numerics. In the following we list the various predictions for the differential cross section (74) that are displayed together with the HERMES measurements [30] in Fig. 8, where statistical and systematical errors are added in quadrature (same applies for Fig. 9 and Fig. 10). In the confrontation of model predictions and measurements we should bear in mind that at small $-t' \lesssim 0.5\,\mathrm{GeV}^2$ the longitudinal cross section should dominate and that the large $-t'$ region, in which the neglected transverse cross section plays a role, is a priory not suited for the collinear factorization approach.

dotted: *pion pole and* $\widetilde{H} = 0$*, running coupling*

We recall first the model prediction that relies on an overwhelming role of the pion pole, shown in Fig. 4 of Ref. [30] as dot-dashed curve. We imitate this model by setting $\widetilde{H}$ GPD to zero and replacing $\widetilde{\mathcal{E}}$ by its real part within the parameter set (57), see also left panel in Fig. 7. The resulting cross section is plotted in Fig. 8 as dotted line, which resembles the corresponding curve in Fig. 4 of Ref. [30]. As one realizes the model fails to describe the normalization of the cross section at very low $-\langle t'\rangle \sim 0.08\,\mathrm{GeV}^2$, where the discrepancy can reach one order of magnitude at larger $\mathcal{Q}^2$ values. Since Regge-inspired model estimates [33, 35], e.g., compare dashed and dotted curves in Fig. 4 of Ref. [30], state that the $1/R$ ratio should be close to zero at $t' = 0$, a popular conclusion drawn from the observation is that so-called "power contributions" are needed.

dashed: *pion pole and minimalist* $\widetilde{H}$ *model, running coupling*

We take now the same model for $\widetilde{\mathcal{E}}$ as above and include the $\widetilde{H}$ GPD within the parameter set (45), displayed as dashed line. As expected from our considerations in Sect. 3.4, the inclusion of $\widetilde{H}$ yields a flatter t-dependence, compare dashed with dotted curves. One also realizes that for the lowest $x_{\rm B}$ values (left panel), which means also low $\langle \mathcal{Q}^2 \rangle = 1.4\,{\rm GeV}^2$, the cross section at small $-t'$ increase by roughly a factor of two and so the discrepancy of model estimate and measurement diminish, see also the left panel in Fig. 7. However, the discrepancy increases with growing $\mathcal{Q}^2$ and reaches approximately one order of magnitude at $\langle \mathcal{Q}^2 \rangle = 5.4\,{\rm GeV}^2$. Since the LO prediction of the cross section is proportional to the square of the running coupling (9), its normalization changes within the canonical scale setting prescription for the renormalization scale $\mu_R = \mathcal{Q}$ by

$$\frac{d\sigma^{\gamma^* p \to n\pi^+}(x_{\rm B}, t, \mathcal{Q}^2 = 5.4\,{\rm GeV}^2)}{d\sigma^{\gamma^* p \to n\pi^+}(x_{\rm B}, t, \mathcal{Q}^2 = 1.4\,{\rm GeV}^2)} \sim \frac{\alpha_s^2(\mathcal{Q}^2 = 5.4\,{\rm GeV}^2)}{\alpha_s^2(\mathcal{Q}^2 = 1.4\,{\rm GeV}^2)} \approx 0.5\,.$$

Hence, we might be tempted to conclude that half of the discrepancy, observed at $\mathcal{Q}^2 = 5.4\,{\rm GeV}^2$, arises from logarithmic scaling violation, mainly induced by the running coupling.

dot-dashed: *pion trajectory $\widetilde{E}$ model (57) and minimalist $\widetilde{H}$ model, frozen coupling*

If we now freeze the coupling (79), our model with reggeized pion pole ($\Im{\rm m}\widetilde{\mathcal{E}} \neq 0$), describes data rather well at smaller $-t'$ values, see dot-dashed curve. The growing discrepancy within increasing $-t'$ might be understood as an increase of the transverse cross section. Indeed, the dot-dashed curve is rather close to the Regge model prediction [33] for the longitudinal cross section, shown in Fig. 4 of Ref. [30] as dotted curve, while the prediction for the full differential cross section, shown there as dashed curve, matches the experimental measurements. Hence, if one would borrow the $1/R$ ratio from the Regge-inspired model, we would presumably conclude that our GPD model describes data over an astonishing large $|t'|$ range.

dot-dot-dashed: *pion trajectory $\widetilde{E}$ model (56) and minimalist $\widetilde{H}$, frozen coupling*

Unfortunately, the parameter set (57) is rather disfavored by lattice data, see dashed curve in the right panel of Fig. 5. Moreover, as we will see below in Fig. 10, it predicts that the single transverse proton spin asymmetry is of order -1 and so it might be considered as ruled out. Taking the parameter set (56), which is more favored by lattice simulations, we obtain the dot-dot-dashed curve in Fig. 8. Now the discrepancy of the normalization at small t' increases again with growing $\mathcal{Q}^2$. Note also that the t'-dependence is now flatter and if we would correct the normalization for large value of $\mathcal{Q}^2$ in the right panel, the model would perfectly describe data. In other words our model description would then state that the cross section is dominated by the longitudinal part of the cross section over a large lever arm in $-t$. This would then contradict the Regge-inspired model predictions [33, 35].

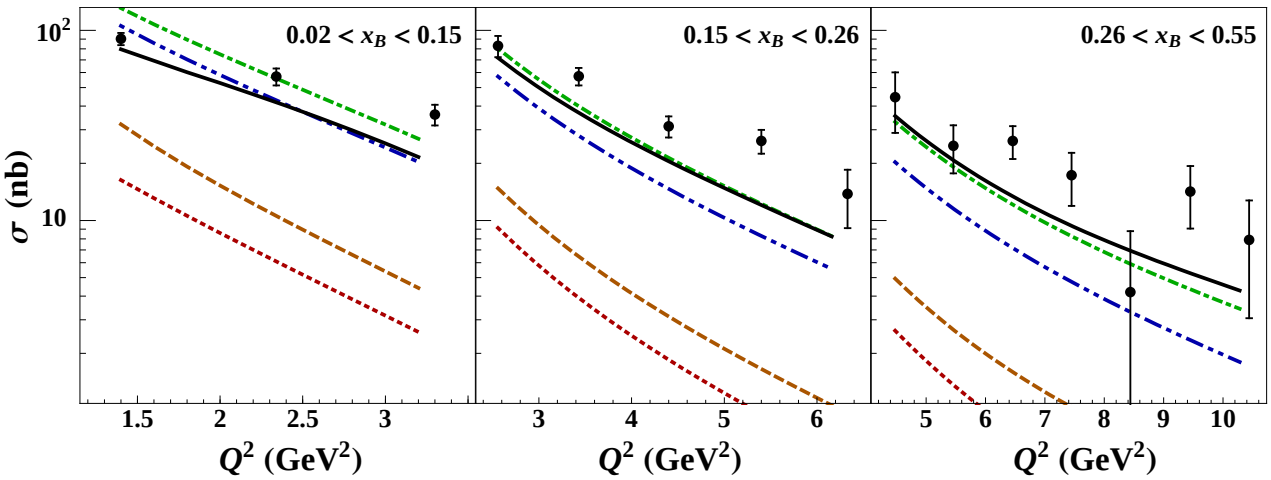

Figure 9: Total cross section $\sigma^{\gamma^* p\to n\pi^+}$ versus $\mathcal{Q}^2$ measurements from HERMES [30] are shown together with a tuned (solid) and various ad hoc GPD model estimates with $1/R = 0$. Same models as in Fig. 8.

solid curve: *pion trajectory $\widetilde{E}$ model (57) and tuning $\widetilde{H}$, frozen coupling*

As we demonstrated, our minimalist GPD models provide us with a variety of predictions and confronting them with experimental data might imply contradictory conclusions about the failure or successes of the collinear factorization approach. Hence, as advocated in Ref. [29], it is more appropriate to change the GPD approach. We now assume that the collinear factorization approach with a frozen coupling works and ask now for the functional form of the GPD at its cross-over trajectory, which entirely determines the imaginary and real part of CFFs to LO accuracy. Instead of introducing a new parameterization for GPDs on the cross-over line we employ here the Mellin-Barnes integral again. Only for illustration we consider it as representation for a complex valued function, satisfying the dispersion relations (60) and (61), where the physical/partonic meaning of the parameters is mostly lost. From an "eye fit", where we already included preliminary HERMES data for the single transverse proton spin, we find that the parameters set

$$\begin{aligned} &\widetilde{h}^{\text{val}}\ \text{“fit”}\ 0.98\,,\quad \beta^{\text{val}}_{\widetilde{H}}\ \text{“fit”}\ 3/2\,,\quad \delta\beta^{\text{val}}\ \text{“fit”}\ 1/2\,, \qquad \widetilde{h}^{\text{sea}}\ \text{“fit”}\ 1\,,\quad \beta^{\text{sea}}_{\widetilde{H}}\ \text{“fit”}\ 5\,,\quad \delta\beta^{\text{sea}}\ \text{“fit”}\ 1\,, \\ &\widetilde{e}^{\text{val}}\ \text{“fit”}\ 0\,,\qquad \beta^{\text{val}}_{\widetilde{E}}\ \text{“fit”}\ 1\,, \qquad\qquad\qquad\qquad\qquad\quad \widetilde{e}^{\text{sea}}\ \text{“fit”}\ 0\,,\quad \beta^{\text{sea}}_{\widetilde{E}}\ \text{“fit”}\ 3 \end{aligned} \tag{80}$$

will lead to a good description of data. In Fig. 8 we realize that the solid curve indeed describes the small $-t'$ data points and leaves some space for the contribution of the transverse cross section.

In Fig. 9 we also display our model results for the total cross section $\sigma^{\gamma^* p\to n\pi^+}$ versus $\mathcal{Q}^2$. Such confrontation is sometimes viewed as a test for the onset of the perturbative approach. However, we should also spell out some warnings. First at all, the total cross section $\sigma^{\gamma^* p\to NM}$ is not a

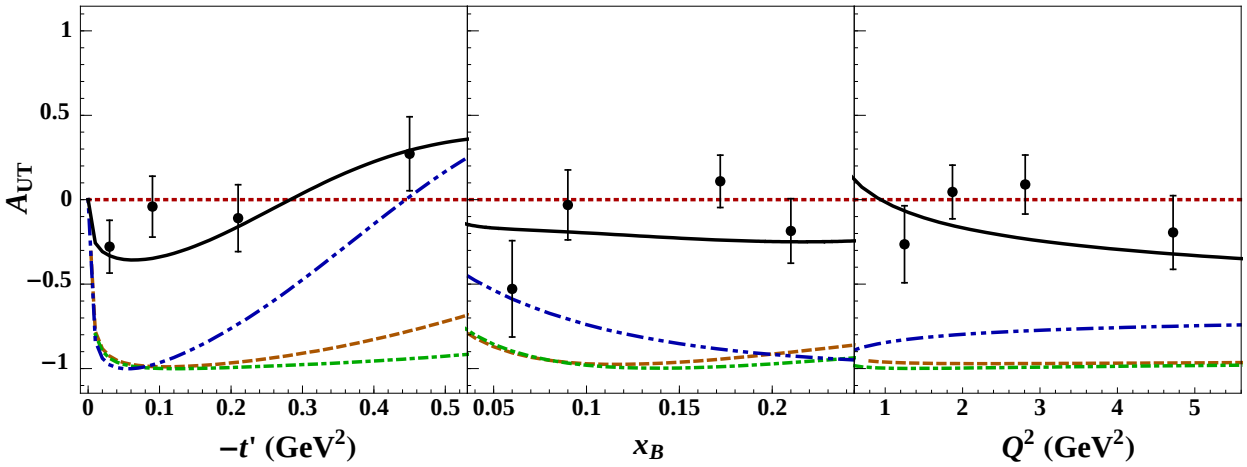

Figure 10: Preliminary HERMES measurements [36] of the single transverse proton spin asymmetry $A_{\rm UT}^{\sin(\phi-\phi_S)}$ versus a tuned (solid) and various ad hoc GPD model predictions, same as in Fig. 8.

pure twist-two quantity and secondly even if we would have a measurement of its longitudinal part $\sigma_L^{\gamma^* p\to NM}$ it contains necessarily contributions that arise from phase space regions for which the collinear factorization approach is perhaps not applicable. Moreover, since the phase space, accessible in experiment, is restricted, the kinematical variables might be even correlated. Naively, one would expect a $1/\mathcal{Q}^6$ scaling and if it would show up in the data one might say that the onset of scaling justifies the perturbative approach. Also the reversed logic has been often stressed in the literature. Certainly, in the first place the running coupling, appearing in the hard amplitude, and also logarithmic scaling violation, predicted by evolution, demolishes this logic and reminds us that logarithmic scaling violations are part of the perturbative framework. Indeed, our two models within running coupling (dotted and dashed) have a steeper $\mathcal{Q}^2$-dependence as the models that were treated with a frozen coupling (dot-dashed, dot-dot-dashed, and solid) and dashed). The $\mathcal{Q}^2$ slope of our "fitted" GPD model prediction (solid) fairly follows the data. That it underestimates the total cross section measurement is natural, since we describe only the differential cross section at smaller $-t'$ values. The differences might arise from the transverse cross section.

We now confront our model predictions in Fig. 10 with a preliminary measurement of the single transverse proton spin asymmetry $A_{\rm UT}^{\sin(\phi-\phi_S)}$, which we describe within the approximation (77). We realize from this formula that the asymmetry is proportional to

$$A_{\rm UT}^{\sin(\phi-\phi_S)} \overset{\rm Tw-2}{\propto} -\Big(\Re{\rm e}\,\widetilde{\mathcal{E}}^{ud}\Big)\Big(\Im{\rm m}\,\widetilde{\mathcal{H}}^{ud}\Big)+\Big(\Im{\rm m}\,\widetilde{\mathcal{E}}^{ud}\Big)\Big(\Re{\rm e}\,\widetilde{\mathcal{H}}^{ud}\Big)\,. \tag{81}$$

For the pure pion pole model (dotted) the asymmetry trivially vanishes. In a pion pole model with non-vanishing $\widetilde{H}$ GPD the asymmetry, shown as dashed curve, is usually predicted to be negative with a large modulus that is rather flat with respect to the t'-dependence; except that it due to the kinematical factor $\sqrt{t'/t_{\rm min}}$ in the asymmetry (77) steeply vanishes at the kinematical

boundary. These characteristic features arise from the fact that the imaginary part of the $\widetilde{\mathcal{H}}$ CFF, equivalently, the $\widetilde{H}$ GPD on the cross-over line, is in all popular GPD models positive and the imaginary part of $\widetilde{\mathcal{E}}$ plays no or not an essential role, see Eq. (81). Obviously, in a twist-two interpretation such standard GPD models [16, 18] are ruled out from the preliminary HERMES measurement [36].

The dot-dot-dashed curve illustrate that the prediction from the reggeized pion pole GPD model in the version (56) looses the characteristic t'-dependence and it can even possess a sign change. In this GPD model the real part of the CFF $\widetilde{\mathcal{E}}$ becomes at larger values of $-t'$ in the vicinity of $x_{\rm B} \sim 0.1$ negative, while $\Im{\rm m}\widetilde{\mathcal{H}}$ remains positive. However, also this twist-two model prediction is still disfavored by experimental data.

If we now give up our minimalist model for the GPD $\widetilde{H}$ and employ the pragmatic parameterization (80), the resulting solid curves are in fair agreement with the experimental points. In this model the real part of $\widetilde{\mathcal{E}}$ is also for larger $-t'$ values positive (in contrast to the dot-dot-dashed model, since we have now $\widetilde{e}^{\rm val} = \widetilde{e}^{\rm sea} = 0$), while now the imaginary part of $\widetilde{\mathcal{H}}$ changes at $-t' \sim 0.3\,{\rm GeV}^2$ the sign and so also the asymmetry. Note also that both terms on the r.h.s. of Eq. (81) are sizeable, where the second term behaves differently than the first one: it is positive at small $-t'$ values and becomes negative at larger $-t'$ values. Thus, also delicate cancellations appear in the asymmetry prediction, which finally determine the shape of the solid curve.

From the confrontation of our GPD models with the transverse target spin asymmetry measurements we conclude that a "predictive power GPD model approach", as it has been emphasized for the overwhelming role of the pion pole, might be misleading. The phase difference between the 'CFF' $\widetilde{\mathcal{H}}$ and $\widetilde{\mathcal{E}}$ are not predictable at larger values of $-t'$. As said before, relying on the twist-two dominance of this observable one can "fit" experimental data to reveal GPDs. Unfortunately, we have also illustrated that rather different GPD model scenarios are potentially able to describe the HERMES measurements.

Finally, we confront in Fig. 11 our models with the measurements of the longitudinal differential cross section $d\sigma_L^{\gamma^* p \to n\pi^+}/dt$ from Hall C collaboration [32], where we do not account for systematical errors. As one realizes also this low energy data are described by the GPD model (80), "fitted" to HERMES data, while all other models underestimate the measurement. In particular, the pion pole model (dotted) with running coupling fails in the normalization and it possesses a too flat t-dependence. Freezing the coupling, the cross section estimate will be roughly enhanced by a factor five and the pion pole model without $\widetilde{H}$ is becoming closer to experimental data. This estimate is similar to our dash-dotted curve, based on the $\widetilde{E}$ parameterization (57). However, we see from the alternative $\widetilde{E}$ parameterization (56), shown as dot-dot-dashed curve, that the model predictions are sensitive to the shape of $\widetilde{E}$ GPD, too. Now the model roughly underestimates

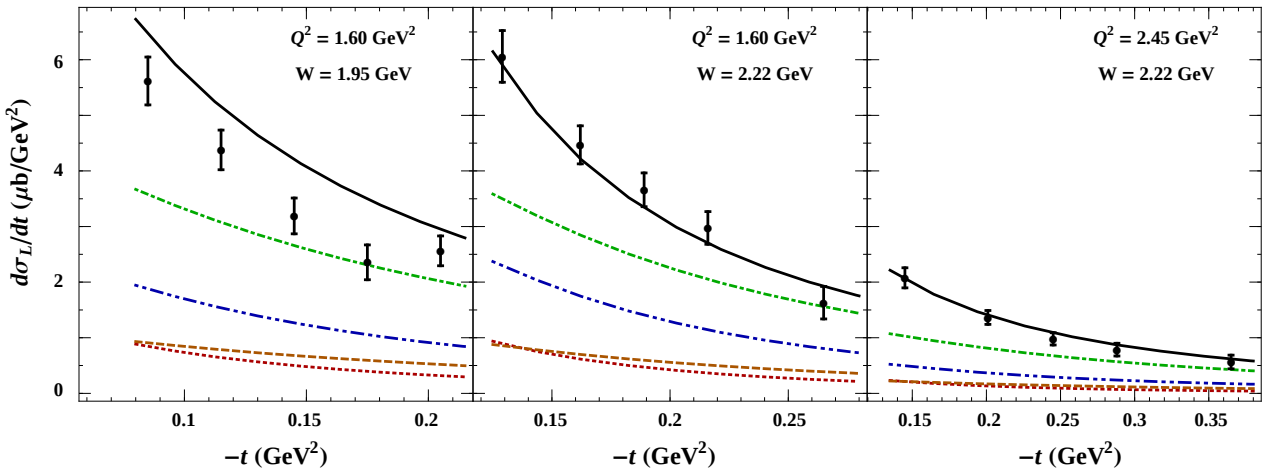

Figure 11: Measurements of the longitudinal differential cross section $d\sigma_L^{\gamma^* p\to n\pi^+}/dt$ in Hall C at JLAB [32] versus various GPD model predictions, same as in Fig. 8. Only statistical errors are included.

experimental data by a factor three. Employing the parameter set (80), we enhance the GPDs in the large x region and describe experimental data. This enhancement feature of cross sections at low energy has been also observed in the hard ρ electroproduction and it was modelled within a D-like addenda [26]. We like to emphasize the intrinsic duality aspect of GPDs that such an enhancement is naturally tied to the GPD behavior on the cross-over line, see also the spectator model [104]. We add that our "fitted" GPD model also describes HALL C data from Ref. [31] and that the VGG plus "power corrections" code [15] is also in fair agreement with HALL C data, too.

5 Summary and conclusions

In this paper we have applied generic GPD modelling [50] to set up zero-skewness $\widetilde{H}$ and $\widetilde{E}$ GPDs in the iso-vector sector. Thereby, we were confronted with the problem that Regge phenomenology within unnatural parity exchanges is challenging. Relying on the restoration of chiral symmetry in hard or even high-energy processes, we conjectured a master trajectory for odd J^{++} exchanges. Such a restoration might be also somehow indicated by the appearance of the $a_3(1875)$ meson, which is listed by the PDG under further states. The hypothetic trajectory naturally explains the rise of the polarized DIS structure function g_1 at smaller $x_{\rm B}$. We illustratively took a SU(6) symmetric valence scenario for the net contribution. In such a scenario the 'spin puzzle' in the iso-vector valence quark sector is trivially resolved. The incorporation of t-dependence in our generic GPD model is based on a Regge pole product ansatz in Mellin space, where the PCAC Ward-

identity could be satisfied within a linear pion trajectory. Both form factor and generalized form factor lattice measurements are then well described. Certainly, the model can be refined, were in accordance with spectroscopic data a non-linear pion trajectory should be taken into account.

Generic arguments to skew a GPD and to find so its value on the cross-over line are only given by large-x counting rules. Compared to the skewness-zero GPD, they are enhanced in the large-x region. Moreover, the skewness dependence of GPDs could be also constrained by precise lattice measurements, expected to be available somewhen in future, however, it is clear that this information is not sufficient to pin down a GPD on the cross-over line. Here we set up ad hoc models within the minimalist skewing prescription in which only the leading SO(3) partial wave in the expansion of conformal moments is taken into account. Our GPD models on the cross-over line possess the expected large-x behavior, however, the suppression of t-dependence for $x \to 1$ might be too weak. More flexible models can be built by including non-leading SO(3) partial waves and they can be tuned to experimental data [49].

To confront the ad hoc GPD models with experimental measurements, we relied on the collinear factorization approach to LO accuracy. Thereby, perturbative corrections were taken qualitatively into account by incorporating them in the coupling via the BLM scale setting prescription. This might to some extent cure the perturbative approach. However, the coupling itself is now considered as a *non-perturbative* expansion parameter that must be fixed from experimental data, too. In such a procedure it is rather likely that the coupling looses its universality and it should be rather considered as an effective one. Nevertheless, we end up with a semi-quantitative framework for the GPD phenomenology that can be tested versus experimental measurements.

We demonstrated then that the hard π^+ production cross section for HERMES kinematics at small $-t'$ can be described within our minimalist GPD models. Thereby, the $\widetilde{H}$ GPD is important, too, and so the pion pole in the $\widetilde{E}$ GPD plays an essential, however, not an overwhelming role. We also considered the single transverse proton spin asymmetry, preliminarily measured by the HERMES collaboration, where we assumed that power suppressed contaminations, induced by the exchange of transverse polarized photons, are small. For small $-t'$ values the sign of the asymmetry is determined by both the pion pole and the sign of the $\widetilde{H}$ GPD on the cross-over line. In our ad hoc models the sign of both contributions is positive, in agreement with the experimental findings. However, or ad-hoc models are now disfavored for larger $-t'$ values, where they predict as other popular models a large negative asymmetry. Tuning the GPDs on the cross-over line, we were able to describe the measurements, too. For larger $-t'$ the pion pole is not overwhelming and the relative phase between $\widetilde{\mathcal{H}}$ and $\widetilde{\mathcal{E}}$ 'CFFs' has an intricate variable dependence, which can hardly be predicted. In our perturbative framework the same ad hoc models are also disfavored by the longitudinal photoproduction cross section measurements in HALL C at JLAB.

Our phenomenological studies illuminated the problems in the extraction of GPDs from hard exclusive meson electroproduction measurements. Finally, let us clearly spell out the challenges. On one hand GPDs are intricate functions, depending on the momentum fraction, the skewness parameter, and the momentum transfer squared. Thus, one can not expect that popular GPD models, which we mainly consider to be ad hoc, are able to describe experimental data. This problem[7] can be resolved within flexible GPD models used in robust numerical fitting routines [45, 49]. So far this approach has been applied to deeply virtual Compton scattering in the small-$x_{\rm B}$ region and within 'dispersion relation' technique for fixed target kinematics [49]. Indeed, such an approach allowed for the first time to access the H GPD at leading order and revealed so the failure of ad hoc models, used before. We emphasize that for the hard exclusive meson electroproduction the theoretical framework is not well understood. To judge on the collinear factorization approach and its improvements, one can utilize the universality of GPDs. Namely, from a widely phenomenological application of the GPD approach within flexible GPD models or 'dispersion relations' one might test its internal consistency. If such a phenomenological consistency check is successful, one simultaneously reveals the GPDs, mainly on the cross-over line.

Acknowledgements

D.M. is grateful to K. Kumerički and K. Passek-Kumerički for the collaboration in generic modelling of parity-even GPDs, where the framework has been adopted here to the parity-odd sector. We are indebted to I. Hristova for providing us preliminary HERMES data and to J. M. Laget for numerical model results. For discussions on Regge and model aspects we thank S. S. Afonin, M. Polyakov, M. Guidal, and P. Kroll.

First note added

During the preparation of the manuscript we were becoming aware of (preliminary) photon-to-pion transition form factor measurements from the BaBar collaboration, which are now available in Ref. [128]. These experimental data do not support the canonical scaling, which we have implicitly assumed, to fix the inverse moment of the pion distribution amplitude. They challenge our interpretation of the connection among photon-to-pion form factor, pion form factor, and hard exclusive π^+ electroproduction, however, the normalization of our numerical results is essentially adopted from the pion form factor. Nevertheless, the BaBar measurement [128] yield a 'crisis' for the perturbative description of pion related processes and the present understanding of the

[7] Alternatively, one might first ask for the value of CFFs by utilizing analytic formulae [10, 41] or fitter codes [126, 127], where the later method is accomplished with error estimates.

partonic substructure of the pion. First comments and interpretations of the BaBar measurement are given in Refs. [122, 129, 130]. Since the pion-to-photon transition form factor is a key process for a QCD understanding, we would like to encourage the BELLE collaboration to cross check the measurement and we recall that a double tagged experiment might provide a deeper insight into the 'pion crisis'. We add that the theoretical description of all exclusive B decay into pion channels is affected by this 'crisis'.

Second note added

After our manuscript was essentially finished, S.V. Goloskokov and P. Kroll submitted their work *An attempt to understand exclusive π^+ electroproduction* [131]. The authors rely on a 'hand-bag' approach, which can be considered as a model improved collinear GPD approach. The advantage of such an approach is that various observables can be successfully described, which provides some trust in the underlying GPD framework. We try to stay as close as possible to the collinear factorization approach in the hope that GPD universality and a systematical improvement can be ensured in a maximal manner. This we consider as a requirement that allows aiming for the primary goal, namely, to reveal GPDs from experimental measurements.

References

[1] J. Collins, L. Frankfurt and M. Strikman, Phys. Rev. **D56**, 2982 (1997), [hep-ph/9611433].

[2] D. Müller, D. Robaschik, B. Geyer, F.-M. Dittes and J. Hořejši, Fortschr. Phys. **42**, 101 (1994), [hep-ph/9812448].

[3] A. V. Radyushkin, Phys. Lett. **B380**, 417 (1996), [hep-ph/9604317].

[4] X. Ji, Phys. Rev. **D55**, 7114 (1997), [hep-ph/9609381].

[5] G. Lepage and S. Brodsky, Phys. Rev. **D22**, 2157 (1980).

[6] A. Efremov and A. Radyushkin, Phys. Lett. **B94**, 245 (1980).

[7] M. Diehl, Phys. Rept. **388**, 41 (2003), [hep-ph/0307382].

[8] A. V. Belitsky and A. V. Radyushkin, Phys. Rept. **418**, 1 (2005), [hep-ph/0504030].

[9] O. V. Teryaev, Analytic properties of hard exclusive amplitudes, 2005, hep-ph/0510031, hep-ph/0510031.

[10] A. V. Belitsky, D. Müller and A. Kirchner, Nucl. Phys. **B629**, 323 (2002), [hep-ph/0112108].

[11] A. V. Radyushkin, Phys. Lett. **B385**, 333 (1996), [hep-ph/9605431].

[12] L. Mankiewicz, G. Piller and T. Weigl, Eur. Phys. J. **C5**, 119 (1998), [hep-ph/9711227].

[13] L. Mankiewicz, G. Piller and T. Weigl, Phys. Rev. **D59**, 017501 (1999), [hep-ph/9712508].

[14] L. Mankiewicz, G. Piller and A. Radyushkin, Eur. Phys. J. **C 10**, 307 (1999), [hep-ph/9812467].

[15] M. Vanderhaeghen, P. A. M. Guichon and M. Guidal, Phys. Rev. **D60**, 094017 (1999), [hep-ph/9905372].

[16] L. L. Frankfurt, P. V. Pobylitsa, M. V. Polyakov and M. Strikman, Phys. Rev. **D60**, 0140010 (1999), [hep-ph/9901429].

[17] L. L. Frankfurt, M. V. Polyakov, M. Strikman and M. Vanderhaeghen, Phys. Rev. Lett. **84**, 2589 (2000), [hep-ph/9911381].

[18] A. V. Belitsky and D. Müller, Phys. Lett. **B513**, 349 (2001), [hep-ph/0105046].

[19] D. Y. Ivanov, L. Szymanowski and G. Krasnikov, JETP Lett. **80**, 226 (2004), [hep-ph/0407207], Pisma Zh. Eksp. Teor. Fiz 80 (2004) 255.

[20] A. V. Belitsky, A. Freund and D. Müller, Nucl. Phys. **B574**, 347 (2000), [hep-ph/9912379].

[21] L. Mankiewicz and G. Piller, Phys. Rev. **D61**, 074013 (2000), [hep-ph/9905287].

[22] N. Kivel, Phys. Rev. **D65**, 054010 (2002), [hep-ph/0107275].

[23] N. Kivel, AIP Conf. Proc. **775**, 81 (2005).

[24] I. V. Anikin, D. Y. Ivanov, B. Pire, L. Szymanowski and S. Wallon, QCD factorization beyond leading twist in exclusive rho(T) meson production, 2009, 0904.1482.

[25] M. Diehl and W. Kugler, Eur. Phys. J. **C52**, 933 (2007), [0708.1121].

[26] M. Guidal and S. Morrow, Exclusive ρ^0 electroproduction on the proton: GPDs or not GPDs?, 0711.3743 [hep-ph], 2007.

[27] S. V. Goloskokov and P. Kroll, Eur. Phys. J. **C42**, 281 (2005), [hep-ph/0501242].

[28] S. V. Goloskokov and P. Kroll, Eur. Phys. J. **C53**, 367 (2008), [0708.3569].

[29] K. Kumerički, D. Müller and K. Passek-Kumerički, Eur. Phys. J. **C58**, 193 (2008), [0805.0152].

[30] HERMES, A. Airapetian *et al.*, Phys. Lett. **B659**, 486 (2008), [0707.0222].

[31] T. Horn *et al.*, Phys. Rev. **C78**, 058201 (2008), [0707.1794].

[32] Jefferson Lab, H. P. Blok *et al.*, Phys. Rev. **C78**, 045202 (2008), [0809.3161].

[33] M. Guidal, J. M. Laget and M. Vanderhaeghen, Nucl. Phys. **A627**, 645 (1997).

[34] M. M. Kaskulov, K. Gallmeister and U. Mosel, Deeply inelastic pions in the exclusive reaction $p(e, e'\pi^+)n$ above the resonance region, 2008, 0804.1834.

[35] M. M. Kaskulov and U. Mosel, Deep exclusive electroproduction of π^+ at HERMES, 2009, 0904.4442.

[36] I. Hristova, (for the HERMES collaboration), Proc. of the XVI Int. Workshop on Deep Inelastic Scattering and Related Topics (DIS 2008), London, England, 7-11 Apr 2008 [doi:10.3360/dis.2008.95].

[37] S. J. Brodsky, M. Burkardt and I. Schmidt, Nucl. Phys. **B441**, 197 (1995), [hep-ph/9401328].

[38] M. V. Polyakov, Nucl. Phys. **B555**, 231 (1999), [hep-ph/9809483].

[39] X.-D. Ji and R. F. Lebed, Phys. Rev. **D63**, 076005 (2001), [hep-ph/0012160].

[40] A. Bacchetta, U. D'Alesio, M. Diehl and C. A. Miller, Phys. Rev. **D70**, 117504 (2004), [hep-ph/0410050].

[41] A. V. Belitsky and D. Müller, Phys. Rev. **D79**, 014017 (2009), [0809.2890].

[42] D. Müller, Phys. Rev. **D59**, 116003 (1999), [hep-ph/9812490].

[43] V. M. Braun, G. P. Korchemsky and D. Müller, Prog. Part. Nucl. Phys. **51**, 311 (2003), [hep-ph/0306057].

[44] D. Müller and A. Schäfer, Nucl. Phys. **B739**, 1 (2006), [hep-ph/0509204].

[45] K. Kumerički, D. Müller and K. Passek-Kumerički, Nucl. Phys. B **794**, 244 (2008), [hep-ph/0703179].

[46] J. R. Cudell, A. Donnachie and P. V. Landshoff, Phys. Lett. **B448**, 281 (1999), [hep-ph/9901222].

[47] M. Diehl, T. Feldmann, R. Jakob and P. Kroll, Eur. Phys. J. **C39**, 1 (2005), [hep-ph/0408173].

[48] M. Guidal, M. V. Polyakov, A. V. Radyushkin and M. Vanderhaeghen, Phys. Rev. **D72**, 054013 (2005), [hep-ph/0410251].

[49] K. Kumericki and D. Mueller, Deeply virtual Compton scattering at small x_B and the access to the GPD H, 2009, 0904.0458.

[50] D. Müller, K. Kumericki and K. Passek-Kumericki, GPD sum rules: a tool to reveal the quark angular momentum, 0807.0170, 2008.

[51] Particle Data Group, C. Amsler *et al.*, Phys. Lett. **B667**, 1 (2008).

[52] A. C. Irving and R. P. Worden, Phys. Rept. **34**, 117 (1977).

[53] P. D. B. Collins, *An Introduction to Regge Theory and High Energy Physics* (Cambridge University Press, Cambridge, 1977).

[54] D. V. Bugg, Phys. Rept. **397**, 257 (2004), [hep-ex/0412045].

[55] E. Klempt and A. Zaitsev, Phys. Rept. **454**, 1 (2007), [0708.4016].

[56] J. R. Ellis and M. Karliner, Phys. Lett. **B213**, 73 (1988).

[57] S. S. Afonin, Evidence for new baryon like symmetries in meson spectrum, 2007.

[58] S. S. Afonin, Int. J. Mod. Phys. **A22**, 4537 (2007), [0704.1639].

[59] E. S. Swanson, Phys. Lett. **B582**, 167 (2004), [hep-ph/0309296].

[60] S. U. Chung *et al.*, Phys. Rev. **D65**, 072001 (2002).

[61] S. D. Bass, Rev. Mod. Phys. **77**, 1257 (2005), [hep-ph/0411005].

[62] S. E. Kuhn, J. P. Chen and E. Leader, 0812.3535.

[63] J. Bartels, B. I. Ermolaev and M. G. Ryskin, Z. Phys. **C70**, 273 (1996), [hep-ph/9507271].

[64] R. L. Heimann, Nucl. Phys. **B64**, 429 (1973).

[65] A. V. Anisovich *et al.*, Phys. Lett. **B517**, 261 (2001).

[66] M. Gluck and E. Reya, Nucl. Phys. **B130**, 76 (1977).

[67] D. Diakonov, V. Petrov, P. Pobylitsa, M. V. Polyakov and C. Weiss, Nucl. Phys. **B480**, 341 (1996), [hep-ph/9606314].

[68] M. Wakamatsu and T. Kubota, Phys. Rev. **D60**, 034020 (1999), [hep-ph/9809443].

[69] B. Dressler *et al.*, Eur. Phys. J. **C18**, 719 (2001), [hep-ph/9910464].

[70] K. Goeke, P. V. Pobylitsa, M. V. Polyakov, P. Schweitzer and D. Urbano, Acta Phys. Polon. **B32**, 1201 (2001), [hep-ph/0001272].

[71] M. Wakamatsu, Phys. Rev. **D67**, 034005 (2003).

[72] R. J. Fries and A. Schafer, Phys. Lett. **B443**, 40 (1998), [hep-ph/9805509].

[73] K. G. Boreskov and A. B. Kaidalov, Eur. Phys. J. **C10**, 143 (1999), [hep-ph/9809398].

[74] S. Kumano and M. Miyama, Phys. Rev. **D65**, 034012 (2002), [hep-ph/0110097].

[75] F.-G. Cao and A. I. Signal, Eur. Phys. J. **C21**, 105 (2001), [hep-ph/0103113].

[76] R. Blankenbecler and S. J. Brodsky, Phys. Rev. **D10**, 2973 (1974).

[77] J. F. Gunion, Phys. Rev. **D10**, 242 (1974).

[78] S. D. Bass and P. V. Landshoff, Phys. Lett. **B336**, 537 (1994), [hep-ph/9406350].

[79] HERMES, A. Airapetian *et al.*, Phys. Rev. **D75**, 012007 (2007), [hep-ex/0609039].

[80] HERMES, A. Airapetian *et al.*, Phys. Rev. **D71**, 012003 (2005), [hep-ex/0407032].

[81] T. Gehrmann and W. J. Stirling, Phys. Rev. **D53**, 6100 (1996), [hep-ph/9512406].

[82] J. Blümlein and H. Bottcher, Nucl. Phys. **B636**, 225 (2002), [hep-ph/0203155].

[83] M. Gluck, E. Reya, M. Stratmann and W. Vogelsang, Phys. Rev. **D63**, 094005 (2001), [hep-ph/0011215].

[84] D. de Florian, R. Sassot, M. Stratmann and W. Vogelsang, 0904.3821.

[85] D. de Florian, G. A. Navarro and R. Sassot, Phys. Rev. **D71**, 094018 (2005), [hep-ph/0504155].

[86] LHPC and SESAM, P. Hägler *et al.*, Phys. Rev. **D68**, 034505 (2003), [hep-lat/0304018].

[87] QCDSF, M. Göckeler *et al.*, Phys. Rev. Lett. **92**, 042002 (2004), [hep-ph/0304249].

[88] S. D. Drell and T.-M. Yan, Phys. Rev. Lett. **24**, 181 (1970).

[89] LHPC, P. Hägler *et al.*, Phys. Rev. **D77**, 094502 (2008), [0705.4295].

[90] A1, A. Liesenfeld *et al.*, Phys. Lett. **B468**, 20 (1999), [nucl-ex/9911003].

[91] M. L. Goldberger and S. B. Treiman, Phys. Rev. **110**, 1178 (1958).

[92] S. Choi *et al.*, Phys. Rev. Lett. **71**, 3927 (1993).

[93] A. G. Shuvaev, Phys. Rev. **D60**, 116005 (1999), [hep-ph/9902318].

[94] A. G. Shuvaev, K. J. Golec-Biernat, A. D. Martin and M. G. Ryskin, Phys. Rev. **D60**, 014015 (1999), [hep-ph/9902410].

[95] M. V. Polyakov and K. M. Semenov-Tian-Shansky, Dual parametrization of GPDs versus double distribution Ansatz, 0811.2901, 2008.

[96] Y. L. Luke, *The Special Functions and their Approximations Vol. 1.* (Academic Press New York and London, 1969).

[97] M. V. Polyakov, Phys. Lett. **B659**, 542 (2008), [0707.2509 [hep-ph]].

[98] A. V. Radyushkin, Phys. Lett. **B449**, 81 (1999), [hep-ph/9810466].

[99] F. Yuan, Phys. Rev. **D69**, 051501 (2004), [hep-ph/0311288].

[100] M. Burkardt, Phys. Lett. **B595**, 245 (2004), [hep-ph/0401159].

[101] M. Burkardt, GPDs with $\zeta \neq 0$, 2007, 0711.1881.

[102] A. Mukherjee, I. V. Musatov, H. C. Pauli and A. V. Radyushkin, Phys. Rev. **D67**, 073014 (2003), [hep-ph/0205315].

[103] B. C. Tiburzi, W. Detmold and G. A. Miller, Phys. Rev. **D70**, 093008 (2004), [hep-ph/0408365].

[104] D. S. Hwang and D. Müller, Phys. Lett. **B660**, 350 (2008), [0710.1567].

[105] M. Penttinen, M. V. Polyakov and K. Goeke, Phys. Rev. **D62**, 014024 (2000), [hep-ph/9909489].

[106] M. V. Polyakov and C. Weiss, Phys. Rev. **D60**, 114017 (1999), [hep-ph/9902451].

[107] A. V. Belitsky, X.-d. Ji and F. Yuan, Phys. Rev. Lett. **91**, 092003 (2003), [hep-ph/0212351].

[108] M. Diehl and S. Sapeta, Eur. Phys. J. **C41**, 515 (2005), [hep-ph/0503023].

[109] N. Isgur and C. L. Smith, Nucl. Phys. **B317**, 526 (1989).

[110] A. Radyushkin, Nucl. Phys. **A532**, 141 (1991).

[111] H.-N. Li and G. Sterman, Nucl. Phys. **B381**, 129 (1992).

[112] R. Jakob and P. Kroll, Phys. Lett. **B315**, 463 (1993), [hep-ph/9306259], Phys. Lett. B319, 545 (E) (1993).

[113] S. J. Brodsky, C.-R. Ji, A. Pang and D. G. Robertson, Phys. Rev. **D57**, 245 (1998), [hep-ph/9705221].

[114] V. M. Braun, A. Khodjamirian and M. Maul, Phys. Rev. **D61**, 073004 (2000), [hep-ph/9907495].

[115] A. V. Belitsky, D. Müller, L. Niedermeier and A. Schäfer, Phys. Lett. **B474**, 163 (2000), [hep-ph/9908337].

[116] S. Brodsky, G. Lepage and P. Mackenzie, Phys. Rev. **D28**, 228 (1983).

[117] S. J. Brodsky and F. J. Llanes-Estrada, Eur. Phys. J. **C46**, 751 (2006), [hep-ph/0512247].

[118] I. V. Anikin, B. Pire, L. Szymanowski, O. V. Teryaev and S. Wallon, Phys. Rev. **D70**, 011501 (2004), [hep-ph/0401130].

[119] B. Melić, B. Nižić and K. Passek, Phys. Rev. **D65**, 053020 (2002), [hep-ph/0107295].

[120] CLEO, J. Gronberg *et al.*, Phys. Rev. **D57**, 33 (1998).

[121] I. Musatov and A. Radyushkin, Phys. Rev. **D56**, 2713 (1997), [hep-ph/9702443].

[122] S. V. Mikhailov and N. G. Stefanis, Transition form factors of the pion in light-cone QCD sum rules with next-to-next-to-leading order contributions, 2009, 0905.4004.

[123] A. P. Bakulev, S. V. Mikhailov and N. G. Stefanis, Phys. Lett. **B508**, 279 (2001), [hep-ph/0103119], Erratum-ibid.B590:309-310,2004.

[124] A. P. Bakulev, S. V. Mikhailov and N. G. Stefanis, Phys. Rev. **D73**, 056002 (2006), [hep-ph/0512119].

[125] Jefferson Lab, G. M. Huber *et al.*, Phys. Rev. **C78**, 045203 (2008), [0809.3052].

[126] M. Guidal, Eur. Phys. J. **A37**, 319 (2008), [0807.2355].

[127] M. Guidal and H. Moutarde, Generalized Parton Distributions from Deeply Virtual Compton Scattering at HERMES, 2009, 0905.1220.

[128] BaBaR coll., B. Aubert *et al.*, Measurement of the $\gamma\gamma^* \to \pi^0$ transition form factor, 2009, 0905.4778.

[129] A. V. Radyushkin, Shape of Pion Distribution Amplitude, 2009, 0906.0323.

[130] M. V. Polyakov, On the Pion Distribution Amplitude Shape, 2009, 0906.0538.

[131] S. V. Goloskokov and P. Kroll, An attempt to understand exclusive π^+ electroproduction, 2009, 0906.0460.